Intervertebral disc cells from human back pain subjects exhibit TNFR1-mediated senescence and lack TNFR2-modulated repair capacity

Jennifer Gansau[1], Elena Grossi[2,3], Levon Rodriguez [1,4], Minghui Wang[4], Damien M. Laudier[1], Saad Chaudhary[1], Andrew C. Hecht[1], Wenyu Fu[5], Robert Sebra[4], Chuanju Liu[5], James C. Iatridis[1,*]

[1]Department of Orthopaedics, Icahn School of Medicine at Mount Sinai; New York, NY 10029, USA.

[2]Department of Oncological Sciences, Icahn School of Medicine at Mount Sinai; New York, NY 10029, USA.

[3]Department of Dermatology, Icahn School of Medicine at Mount Sinai; New York, NY 10029, USA.

[4]Department of Genetics & Genomic Sciences, Icahn School of Medicine at Mount Sinai; New York, NY 10029, USA.

[5]Department of Orthopaedics & Rehabilitation, Yale University School of Medicine; New Haven, CT 06510, USA.

*Corresponding author. James C Iatridis

Email: james.iatridis@mssm.edu

Address: Leni and Peter W. May Department of Orthopaedics

One Gustave Levy Place, Box 1188

Icahn School of Medicine at Mount Sinai

New York, NY 10029, USA

Telephone: +1-212-241-1517

Abstract: Intervertebral disc (IVD) degeneration (IVDD) progresses to herniation and back pain due to the poor IVD healing capacities. However, factors contributing to inferior IVD repair remain to be elucidated. Here we identify distinct roles of TNFα-receptors (TNFRs) in IVD cell responses to back pain conditions as key factors in poor IVD healing responses. IVDD tissue of back pain subjects with herniation secreted a complex array of pro-inflammatory cytokines and chemokines (including IL-6, IL-10, CCL2 and CCL5) collected as IVDD conditioned media (IVDD-CM). Single-cell RNA-sequencing (scRNA-seq) of human IVDD tissues revealed these cytokines were dominantly expressed by a small macrophage-population with surprisingly low expression by native IVD cells. Human annulus fibrosus (hAF) cells from surgical tissue had reduced metabolic rates and underwent senescence in IVDD-CM, whereas Basal media restored mitotic potential. Inhibiting the TNFR1 pathway in hAF cells under IVDD-CM challenge enhanced proliferation and induced pro-inflammatory responses with extensive cytokines and chemokines produced. Surprisingly, modulating the pro-reparative TNFR2 using blocking antibodies or using Atsttrin as TNFR2 activator had no effect on hAF cell transcriptome. We discovered TNFR2 was lacking on hIVD cell membranes using immunostaining and scRNA-seq on human autopsy samples and back pain tissue. The absence of TNFR2 on hIVD cells is a new finding revealing these cells are inherently limited in their repair response to inflammatory challenges. Results point to a TNFR-specific strategy for IVD repair involving TNFR1 inhibition to restore IVD cell metabolism and express chemokines to recruit TNFR2-expressing cells capable of a more robust repair response.

INTRODUCTION

Back and neck pain are leading causes of global disability impacting >100 million adults in the US, leading to missed workdays, massive health care expenditures and contributed to opioid epidemic. The care for patients with both axial neck and back pain represents a tremendous socioeconomical burden in the US and globally (*1-4*). Intervertebral disc (IVD) herniation involving annulus fibrosus (AF) defects is a direct cause of pain and disability that can predispose to IVD degeneration (IVDD) and result in pain and disability (*1, 5, 6*).

Chronic inflammation from IVDD is a strong contributor to progressive degenerative conditions and pain. This is due to the known roles that pro-inflammatory cytokines play in increased matrix catabolism, neurovascular ingrowth into the IVD, and enhanced nociception (*7-14*). Furthermore, infiltration of cytokine-releasing macrophages into the peripheral nervous system and damaged IVD has been observed, suggesting a correlation between immune cell infiltration and discogenic pain (*15*). Tumor necrosis factor-alpha (TNFα) is a key regulator of pro-inflammatory conditions. TNFα promotes interleukin-1 Beta (IL-1β) and interleukin-6 (IL-6) secretion and broadly induces matrix catabolism and nociception (*7-11, 16, 17*). The development of strategies to better manage and promote repair in the chronic pro-inflammatory environment of herniated and degenerated IVDs is a priority that needs further research. While pro-inflammatory cytokines are known to be a chronic contributor to painful IVDD, there is much less known about the source of these cytokines and whether it's possible to shift the catabolic response of IVD cells to a pro-reparative response.

In human clinical trials for IVD herniation with radiculopathy, local and systemic administration of TNFα blocking agents, including infliximab, etanercept and adalimumab, showed some promise for pain reduction but remained inconclusive since trials exhibited broad heterogeneity in effects

and several showed negative findings (*18-24*). While a randomized, double-blinded, placebo-controlled trial of 43 patients with disc herniation found some decrease of average back pain using etanercept compared to placebo after 28 weeks, a randomized, controlled trial that enrolled 40 discectomy patients with disc herniation concordant with radicular pain, found infliximab had similar effects as placebo at 3-month follow-up (*19, 25*). Meanwhile, preclinical animal studies show efficacy with early TNFα blocking with reduced pain and improved IVD degeneration score (*10, 26*). Therefore, TNFα inhibition showed efficacy inhibiting pain and IVDD in preclinical models while human clinical trials had high heterogeneity in efficacy of TNFα blocking agents. The contrast between preclinical animal studies and human clinical trials highlights the need for deeper investigations into the roles of TNFα with a focus on its specific receptors in IVD cell responses.

The two receptors for TNFα signaling transduction are TNFα-receptor 1 (TNFR1), which is implicated in the pro-inflammatory response that promotes tissue catabolism, and TNFα-receptor 2 (TNFR2), which is associated with cell survival and tissue repair/regeneration (*27-30*). Current treatment strategies involve antibody-based inhibition with a high binding affinity for TNFα and therefore actively prevents TNFα from binding to both TNFR1 and TNFR2 receptors (*19, 26, 28, 31, 32*). Modulation of TNFα signaling from a predominantly TNFR1 response to a TNFR2 response using the progranulin derived fusion protein Atsttrin demonstrated efficacy as a therapeutic in osteoarthritis (*33-36*). For IVD repair, Atsttrin significantly improved IVD degeneration score on histology and magnetic resonance imaging (MRI) in a murine $TNFR1^{-/-}$ model, whereas $TNFR2^{-/-}$ mice were not affected by Atsttrin (*37*). This suggests that TNFR2 is critical for the functionality of Atsttrin, but also motivates further studies including the application of Atsttrin as a translational therapeutic strategy in human IVDs.

A human relevant cell culture model system is needed to recapitulate the human IVDD clinical condition and evaluate efficacy of Atsttrin and selective TNFR blocking. A common strategy for simulating IVDD conditions is supplementation of cell culture media with pro-inflammatory cytokines such as TNFα and IL-6 (*38-42*). However, painful human IVDD with herniation is known to involve chronic pro-inflammatory factors beyond TNFα and IL-6 that are collectively responsible for different cellular functions thought to inhibit IVD repair and promote painful responses (*9*).

This study tested the hypotheses that human IVDD involves a complex cytokine mixture that drives IVD cells towards senescence and can be shifted towards a reparative responsive by inhibiting TNFR1 and promoting TNFR2 activity. This study was conducted in multiple parts using human surgical subjects with painful IVDD and herniation, and human IVD samples from autopsy to insure human relevant findings. IVD tissues and cells were evaluated using various techniques including cell culture, bulk RNA-sequencing, single-cell RNA-sequencing (scRNA-seq), histology, and multiplex array. The first part characterized the pro-inflammatory cytokines and cells present in human IVDD from surgical back pain subjects. The cytokines secreted from that tissue were collected as conditioned media (CM) and characterized to contain multiple cytokines and chemokines. scRNA-seq on cells isolated from complex IVDD tissue of human surgical subjects identified that these inflammatory cytokines were expressed in high amounts by very few M1-type macrophages. Next, a novel in vitro human AF (hAF) cell culture model of IVDD was developed using this CM. CM had largest effects on hAF cell metabolic rates by inhibiting cell cycle and promoting senescence. This hAF IVDD cell culture model was used as a drug screening platform to determine effects of TNFR1, TNFR2 and Atsttrin. Anti-TNFR1 (αTNFR1) antibodies on hAF cells with CM prevented senescence and modified hAF

transcriptome to alter hAF cell fate. Anti-TNFR2 (αTNFR2) antibodies or Atsttrin had no effects on hAF cells with CM. The levels of TNFR1 and TNFR2 were evaluated in human IVDs from surgical subjects and autopsy samples. TNFR1 significantly increased with IVDD grade while TNFR2 was present at very low levels and was unchanging with degenerative grade. Low levels of TNFR2 in hAF cells suggest that TNFR1 blocking will better enable hAF cells to adapt to the cytokine challenge of IVDD and promote a stronger repair response.

RESULTS

IVDD CM contains many pro-inflammatory cytokines expressed mostly by macrophages

To characterize the IVDD pro-inflammatory microenvironment, IVD specimen (AF and NP) from 9 human clinical subjects (table S1) were collected and cultured in Basal media for 72 hours under constant agitation, leading to cytokine release and generating CM (Fig. 1A, top). The concentration of different cytokines and chemokines within the human IVDD CM were measured with a human cytokine/chemokine panel 48-plex discovery Assay® Array. CM contained significantly higher concentrations of pro- and anti-inflammatory cytokines (e.g., pro-inflammatory cytokines IL-1β, IL-6, TNFα, and anti-inflammatory cytokines IL-1RA, IL-4, IL-10, IL-13) as well as chemokines (e.g., MIP-1α/CCL3, MIP1β/CCL4, MCP-1/CCL2 and MCP-3/CCL7) than Basal media (Fig. 1B, table S2). To determine the cells producing those cytokines, scRNA-seq was performed on cells isolated from 5 herniated IVD specimen (AF and NP) from 3 subjects undergoing Anterior cervical discectomy and fusion (ADF) procedure (1 male, 2 female) (Fig. 1A bottom, fig. S1A). A dataset of 13,259 cells was analyzed with post-data integration of 3 biological replicates that identified 14 clusters. Clusters were annotated using UniCell Deconvolve, a pre-trained, unbiased, deep learning model system (fig. S1) (*43*). Cell cluster 13 was a small population identified as macrophages

using UniCell and confirmed manually by evaluating expression markers including *CD68*, *CXCL16*, *C1QB* and *CD14* (fig. S2A). While these macrophages represent only 0.16% of the cells of the specimens (fig. S2B), we were surprised that these macrophages were the main cells expressing the genes translating to the cytokines released from the IVDD CM (Fig. 1C and D). More broadly, compared to all other cells, the macrophage cluster contained 217 genes that were significantly upregulated (sorted by $\log_2$(FC) and -$\log_{10}$(false discovery rate)) including the pro-inflammatory gene *IL1B* and the chemoattractant chemokines *CCL3* (*MIP1α*), *CCL3L1* and *CCL4* (*MIP1β*), which emphasized the pro-inflammatory function of the macrophages compared to all other cell clusters (Fig. 1E). Pathway analysis further demonstrated the macrophage cluster marker genes (adjusted p- value ≤ 0.05 and $\log_2$(fold change) ≥ 0.25) involved significantly enriched "TNFα Signaling via NFκB" (Score= 385.8, adj. p-value= 2.27×10^{-13}), "Inflammatory Response" (Score= 123.6, adj. p-value= 5.89×10^{-7}) and "Complement" (Score= 100.3, adj. p-value= 3.22×10^{-6}) (Fig. 1F). Analysis of markers for macrophage polarization, namely *IL1B*, *TLR2* and *CXCL2* for M1 polarization and *CD163*, *MRC1* and *IL10* for M2 polarization, did not show a clear distinction of M1/M2 macrophage populations, however, M1- markers had 2.5-fold greater expression (average of 82%, red dotted line) compared to M2-markers (average of 29%, green dotted line). M1/M2 macrophage polarization marker quantification indicated these cells were polarized in an M1 pro-inflammatory and catabolic phenotype with little conversion to M2 anti-inflammatory and reparative phenotype (Fig. 1G and fig. S2C). The high expression levels of cytokines released in herniated IVDD tissues (Fig. 1C) and M1 polarization of these macrophages suggest they contribute to the cytokine profiles. Overall, we conclude that IVDD tissue from back pain subjects contained a complex 'cocktail' of pro-inflammatory cytokines dominantly expressed by a very small population of M1 macrophages highly enriched for TNFα signaling.

hAF cells cultured in CM maintain a degenerative phenotype with inhibited metabolic rate

Having determined that CM contains a complex variety of cytokines, we next sought to use this IVDD CM to generate an in vitro model system representing the inflammatory microenvironment of IVDD and herniation (Fig. 2). The use of CM is considered more representative than most cell culture models that simulate IVDD using a single cytokine. Furthermore, we developed a 2D culture model that promotes the native elongated phenotype of AF cells, simplifies transport conditions, and enables higher throughput screening of more conditions with relatively fewer cells compared to 3D culture conditions. For hAF cell IVDD model studies, we used CM generated from specimens that were collected and pooled from 9 patients (table S1) for a 2-part study exploring dosing and timing. First, the dosing study used hAF cell cultured for 24 hours in Basal media with increasing CM concentrations (Basal, 25, 50 and 100% CM) (Fig. 2A, "1. Media Dosing"). Increasing CM concentration decreased the number of AF cells visible in culture, suggesting CM inhibited hAF cell proliferation, increased cell cycle arrest or promoted cell death (Fig. 2B). CM dosing also significantly decreased AF cell metabolic activity reflected in MTT assay with consistently decreased relative optical density (rOD) with increasing CM concentration (values normalized to Basal group for each biological replicate). A significant drop of rOD from 0.96 ± 0.04 (25% CM) to 0.71 ± 0.04 (100% CM) was observed ($p<0.0001$) (Fig. 2C), suggesting reduced metabolic rates with increased CM concentration due to resulting either from fewer cells, due to less proliferation, or due to increased cell death.

After seeing the most degenerative response of hAF cells in 100% CM, the next part, the timing study compared AF cells cultured with CM exposure for 24 hours vs. 72 hours using 100% CM (Fig. 2A, "2. Media Timing"). 24-hour CM exposure resulted in reduced cell numbers in concordance with the previous dosing study, and 72-hour CM exposure more drastically decreased

cell numbers alongside a change in cell morphology, including a more granulated appearance of cells and elongated stress fibers (Fig. 2D). The MTT assay showed a significant decrease of rOD using CM at 24 hours and 72 hours compared to Basal ($p<0.0001$) (Fig. 2E), and CM treatment significantly reduced rOD at 72 hours (0.78 ± 0.003) compared to 24 hours (0.88 ± 0.03, $p<0.001$), which indicates more damaging effects with time of the treatment (Fig. 2E). Interestingly, gene expression analysis further indicated increasing damage with TNFRs showing a significant upregulation for both receptors: *TNFRSF1A* and *TNFRSF1B* (genes for TNFR1 and TNFR2, respectively) after 24 hours ($p<0.05$ and $p<0.01$ respectively, Fig. 2F), suggesting active cell responsiveness to CM. Meanwhile, 72 hours of CM treatment caused *TNFRSF1A* to be significantly downregulated compared to Basal ($p<0.01$), and no difference in *TNFRSF1B* expression, suggesting less responsiveness of TNFRs after 72 hours CM treatment which could be related to accumulating effects of CM exposure. This dynamic response is also seen in gene expression of matrix metabolism-related genes, which show a significant down-regulation of *COL1A1* in CM after 24 ($p<0.05$) and 72 hours ($p<0.01$) as well as a significant downregulation of *ADAMTS4* after 24 ($p<0.01$) and 72 hours ($p<0.01$) in CM compared to Basal (fig. S3B), consistent with the inhibited cell metabolism rates. No significant change in pro-inflammatory gene expression was found after the time points investigated (fig. S3C)

TNFR1 blocking altered CM effects while TNFR2 blocking and Atsttrin did not

The hAF cell in vitro model representing IVDD and herniation showed increased *TNFRSF1A* and *TNFRSF1B* expression following CM exposure after 24 hours and suggested distinct roles of TNFRs in response to a pro-inflammatory environment. We therefore used inhibiting antibodies against TNFR1 and TNFR2 to evaluate more specifically the roles of TNFRs in modulating the IVDD CM environment. Inhibiting antibodies for TNFR1 and TNFR2 were independently

supplemented to CM and cultured for 24 hours (10 µg/mL) to specifically inhibit signaling of each TNFR. Additionally, the engineered protein Atsttrin was assessed for its potential as a new therapeutic for IVDD by supplementing it to CM prior to 24 hours treatment of hAF cells (200 ng/mL) (Table 1, Fig. 3A). We found that inhibiting the TNFα signaling pathway through TNFR1 partially rescued hAF cells from a CM challenge with increased cell viability, improved cell morphology, and a highly distinct transcriptomic profile with bulk RNA-seq compared to CM, CM+αTNFR2 and CM+Atsttrin (Figs. 3A-3E). Interestingly, and surprisingly hAF cells treated with CM, αTNFR2 and Atsttrin were identical in terms of viability and transcriptomic profile. CM, αTNFR2 and Atsttrin exhibited more floating dead cell compared to Basal and αTNFR1 (pink arrows, Fig. 3B). MTT validated these findings with a significantly higher rOD of cells receiving αTNFR1 compared to CM ($p<0.05$) and αTNFR2 ($p<0.01$), although it was still significantly reduced compared to Basal (Fig. 3C). Meanwhile CM, αTNFR2 and Atsttrin all had significantly lower rOD compared to Basal (Fig. 3C). However, Atsttrin had rOD that was not significantly different from CM or αTNFR2. Bulk RNA-seq with principal component analysis (PCA) on transcriptome results showed three distinct clusters (Basal, αTNFR1 and the three remaining groups) along the first dimension, indicating different transcriptomes depended on conditions/treatment (Fig. 3D). The green cluster on PCA showed CM, αTNFR2 and Atsttrin exhibited very little variability from treatment group with the majority of variability from donor differences and no difference between the treatment. The top 50 differentially expressed genes (DEGs) visualized in the heatmap confirmed PCA results demonstrating distinct patterns for Basal, αTNFR1 and CM groups and no differences between CM, αTNFR2 and Atsttrin groups (Fig. 3E). Gene expression of *TNFRSF1A* and *TNFRSF1B* for each group showed a significant upregulation of *TNFRSF1A* in CM, αTNFR2 and Atsttrin compared to Basal ($p<0.05$) and αTNFR1 ($p<0.001$),

indicating important upregulation of TNFR2 signaling with CM treatments, and successful blocking by αTNFR1 (Fig. 3F). Interestingly, a significant upregulation of *TNFRSF1B* was observed when blocking TNFR1 compared to all groups (Fig. 3F), suggesting TNFR1 inhibition will significantly upregulate *TNFRSF1B* expression in hAF cells. Surprisingly, transcriptomic profiles on heat maps and volcano plots showed no differences between CM, αTNFR2 or Atsttrin indicating that CM treatment dominated those effects and that TNFR2 modulation had no effect whether treated with αTNFR2 or Atsttrin (fig. S4).

CM downregulated DNA replication and promotes inflammation

Basal, αTNFR1 and CM were analyzed further because of the large transcriptional differences and to discern how TNFR1 modulation shifted the response of hAF cells to the CM challenge. CM greatly affected the transcriptome of hAF cells compared to Basal with 509 significantly downregulated DEGs and 762 upregulated DEGs (Fig. 4A). The most significantly downregulated DEGs were members of the minichromosome maintenance gene family (*MCM* genes), which play a key role in DNA replication (*44*). Gene Set Enrichment Analysis (GSEA) further clarified this finding by showing that CM treatment had the highest scores for depleting pathways related to Cell cycle and DNA replication while inflammatory responses was most significantly enriched, correlating with phenotypic findings (Fig. 4B). The αTNFR1 treatment compared to CM identified 490 DEGs significantly downregulated, and 545 DEGs significantly upregulated (Fig. 4C). GSEA identified these DEGs to be biological processes enriched for IL-27 mediated signaling pathway, which has multiple effects in modulating inflammatory responses (*45*). Additional enriched biological processes were related to Regulation of Neuroinflammatory Response, and Response to Cytokine, demonstrating a shift in the inflammatory pathways activated by CM (Fig. 4D). Interestingly, processes related to Presynaptic Endocytosis and Regulation of Calcium Ion

Dependent Exocytosis were significantly depleted, suggesting That TNFR1 blocking reduces communication with the peripheral nervous system. Blocking TNFR1 showed 448 DEGs significantly downregulated and 1072 DEGs significantly upregulated compared to cells cultured in Basal media, suggesting large transcriptomic differences. The αTNFR1 treatment (which also contained CM) compared to Basal resulted in *NFKB2*, *TNFAIP3* and *CCL5* to be among the most significant and highest FC genes (Fig. 4E), which GSEA demonstrated as significantly enriched biological processes related to cellular response to type 1 interferon, cytokine-mediated signaling pathways, and inflammatory response, while processes related to axonogenesis and axon guidance were significantly depleted (Fig. 4F). Network analysis of DEGs using QIAGEN Ingenuity Pathway Analysis (IPA) further showed a predicted activation of senescence and inhibition of proliferation when hAF cells were cultured in CM (Fig. 4G). On the other hand, when TNFR1 was blocked, processes related to immune cell recruitment were predicted to be activated (Fig. 4H). The activation of an inflammatory response in both comparisons could be further confirmed with IPA.

CM promotes senescence while TNFR1 blocking partially restores cell proliferation

A closer investigation of the cell proliferation and cell cycle between 3 groups was performed since many of the results indicated reduced proliferation and metabolic rates (Fig. 5). CM caused cultured hAF cells to have significant downregulation of genes related to each phase of the cell cycle while Basal upregulated gene markers at each stage in such (Fig. 5B) (*46*). Furthermore, CM caused hAF cells to be express G0 markers indicative of quiescence (i.e., downregulation of *FOXM1*, *BIRC5* and *H2AFZ* and upregulation of *PFDN5* and *RPS14*) (*47*), which may lead to downstream senescence and apoptosis, while Basal had an opposite pattern. Blocking TNFR1 led to a pattern of cell cycle markers between CM and Basal, suggesting a partial recovery of

proliferation. The gene *MKI67*, which is the protein-coding gene for KI67, a proliferation marker, was found to be significantly higher expressed in Basal media cultured hAF cells compared to αTNFR1 ($p<0.05$) and CM ($p<0.0001$), with the αTNFR1 in the middle (Fig. 5C). Further investigation of senescence using SA-β-Gal assay showed significant higher level of SA-β-Gal positive hAF cells in CM compared to αTNFR1 ($p<0.01$) and Basal ($p<0.05$), while there was no significant difference between Basal and αTNFR1 (Fig. 5D and E). Interestingly, apoptosis marker Caspase-3 (Casp3) showed no difference in co-localization of cleaved Casp3 and DAPI using the Pearson's correlation coefficient (PCC) or in fluorescent intensity within the nuclei between groups (Fig. 5F-H). Together, transcriptomic and protein assay results indicated that CM downregulated cell cycle markers and pushed cells towards senescence instead of apoptosis while TNFR1 blocking partially protected and restored cell cycle from senescence and the treated cells were able to mount a robust inflammatory response.

TNFR1 increases with IVDD, while TNFR2 expressed only in macrophages

We further tested the hypothesis that lack of responsiveness of TNFR2 blocking using αTNFR2 antibodies and its activation using Atsttrin was due to little or no TNFR2 signaling in IVD cells using immunohistochemistry (IHC) on human autopsy samples and scRNA-seq on human IVDD samples (Fig. 6). Human IVDs of various degeneration grades (n=14, Rutgers grade 1.3-12) were stained for TNFR1 and TNFR2 respectively and the outer AF (oAF) analyzed using HALO Multiplex module (Fig. 6A). TNFR1 was found in the cell membrane of oAF cells as expected, and the % positive cells for TNFR1 significantly correlated with Rutgers IVDD Grade ($p= 0.0162$, Fig. 6B and C). This significant correlation between TNFR1 protein expression and Rutgers degeneration grade was also found in the inner AF and NP (fig. S5). TNFR2 only showed faint staining within and around the nuclei of oAF cells suggesting little presence of TNFR2 (Fig. 6B).

Furthermore, few cells (around 5% AF cells stained positive) expressed TNFR2 even at these low levels, and the % positive cells for TNFR2 were not affected by Rutgers IVDD grades, which was also seen for the inner AF and NP region (Fig. 6D, fig. S5). Gene expression using scRNA-seq of human IVDD subjects showed *TNFRSF1A* expression throughout all cells, whereas *TNFRSF1B* was not found in hAF cells or any other native IVD cell population (Fig. 6E). Interestingly, *TNFRSF1B* was expressed exclusively in the macrophage population, which had negligible expression for *TNFRSF1A* (Figure 6F). Together, human IVD IHC and IVDD scRNA-seq results highlighted the potential role of TNFR1 in IVDD and supported the hypothesis that native IVD cells involve negligible amounts of TNFR2-induced signaling, which provided an explanation as to why αTNFR2 and Atsttrin treatments do not rescue the effects of the CM challenge.

DISCUSSION

There is an immense clinical need to develop improved therapeutic targets to manage the complex inflammatory conditions in painful IVDD which motivated this work. Here, the pro-senescence response of hAF cells exposed to cytokines is shown and how TNFR1 modulation partly recovers this response, which might enable them to mount a more robust inflammatory response (Fig. 7). Specifically, in this study the cytokines present in IVDDs were characterized followed by improving the understanding of the roles of TNFRs in propagating the IVDD while Atsttrin was tested as a novel therapeutic that promotes TNFR2 and inhibits TNFR1 signaling. We first determined that IVDD CM from human subjects contains elevated levels of 32 (of 44) cytokines, underscoring the importance of considering IVDD to be a complex combination of multiple pro-inflammatory cytokines and chemokines. With so many cytokines present, it was therefore notable that scRNA-seq of human IVD tissue from 3 subjects identified these inflammation-related

cytokines and that they were dominantly expressed by a very small population of macrophages with extremely low levels expressed by native IVD cells. CM from IVDD and herniation subjects had largest effects on reduced hAF cell proliferation measured on MTT metabolic rates that were demonstrated to promote cell cycle arrest and senescence. TNFR1 blocking partially rescued hAF cells from the IVDD CM challenge with improved proliferation and a strong pro-inflammatory response to the CM challenge and suggesting TNFR1 inhibition allowed hAF cells to mount a robust reparative response. Results therefore suggest that rescue of cell cycle with enhanced cell proliferation may be a more important therapeutic target objective than a specific shift towards anabolism. Surprisingly, TNFR2 blocking and Atsttrin had no transcriptomic and proliferative differences from CM treatment alone, counter to our hypothesis that receptor-specific modulation could shift AF cells to a reparative response. Lack of efficacy of TNFR2 blocking and Atsttrin was due to the very small amount of TNFR2 in human IVD cells in culture and immunostaining, further highlighted the low/lack of TNFR2 suggesting hAF cells do not have the epigenetic programs to mount a TNFR2-driven reparative response. We conclude that IVDD involves a complex mixture of macrophage-secreted pro-inflammatory cytokines that must be managed in the treatment of painful human IVDD. While very low levels of TNFR2 in human IVD cells suggest that Atsttrin and other strategies promoting TNFR2 agonism are not likely to be successful in promoting hAF cell regeneration in vitro, TNFR1 blocking partially restored hAF cell proliferation to mount a repair response emphasizing that future strategies for promoting AF regeneration should prioritize TNFR1 antagonism over TNFR2 agonism.

An important finding of this study is that IVDD tissue from herniation subjects produced a complex combination of several pro-inflammatory cytokines. Results are consistent with the variety of cytokines found with severity of symptomatic IVD herniation regulating multiple

cytokine and chemokine levels and IL-6 playing an important role in painful conditions (*7, 48*). It is particularly interesting that the major effects of these cytokines in CM were reduced IVD cell metabolic rates, arrested cell cycle, and senescence. IVDs have a low cell density with relatively few cells supporting maintenance of a large and dense extracellular matrix so that IVDs have limited healing potential (*49*). IVD cells are adapted to the low oxygen and glucose microenvironment of the IVD, yet IVDD further inhibits nutrient transport and causes metabolite accumulation to create a harsh IVDD microenvironment considered a key factor in the 'frustrated' IVD healing response that stimulates the production of chronic pro-inflammatory conditions (*49-55*). This study builds on that knowledge to show directly that IVDD CM can arrest hAF cell cycle and induce senescence, providing a reason why IVD cells have increased senescence in IVDD. CM from IVDD can also promote neuronal sprouting and calcium signaling in an IVD organ culture model system to promote a painful phenotype (*56, 57*), consistent with GSEA findings of this study. The hAF cells released from the IVDD matrix in Basal media recovered robustly with relatively high metabolic rates and restored cell cycle responses, suggesting IVDD cells have the potential to be rescued under the right conditions if the cytokine mixture can be shifted to a more reparative response.

Interestingly, scRNA-seq identified that only a very small population of macrophages expressed the cytokines detected in the multiplex array, with native IVD cells expressing these cytokines at much lower, or undetectable levels. The macrophages were in a predominantly M1 phenotype and also expressed markers (i.e., *ACP5* and *CTSK*, the genes coding for the proteins TRAP and CATHEPSIN K), suggesting their potential osteoclastic origin (fig. S2D, E) (*58*). The scRNA-seq results from this study were corroborated by immunostaining of human IVDD that demonstrated macrophage infiltration with a predominantly M1 state that does not convert to a reparative M2

polarization state (*51*). Animal models of IVDD suggest that fibroblastic and inflammatory cells can migrate from the endplate into the AF and NP regions to promote fibrotic remodeling (*59*). The scRNA-seq results of the present study are also profound in suggesting that a very small number of macrophages might produce the cytokines measured at such high levels in the multiplex array. Studies showing pro-inflammatory cytokines and neurotrophins expressed by IVD cells using qPCR and RNA-sequencing on bulk tissues do not distinguish cell type expressing these cytokines that cause matrix catabolism and promote neurovascular ingrowth into the IVD (*12, 13*). This scRNA-seq study therefore provides cell-specificity regarding gene expression and highlights that pro-inflammatory cytokines are likely to be produced by IVD cells at much lower levels than macrophages and other immune cells present in the IVD. The cytokines detected in high abundance in IVDD CM using the multiplex array may therefore be produced at high levels by a very small population of macrophage-derived cells. However, the other IVD cells present in higher numbers may also contribute to the cytokine release, albeit at extremely low levels. These results and the broader literature therefore suggest that immune cells in IVDD, which could involve migration from osteoclastic origins, may play an outsize role in IVDD and herniation cytokine responses.

CM was used to establish and characterize an in vitro hAF cell IVDD model in this study that was capable of promoting and maintaining an IVDD phenotype. A promising finding is that hAF cells released from their IVDD matrix and exposed to a nutrient-rich Basal media environment augment their proliferative capacity and increase their metabolic activity. It has been shown that IVD extracellular matrix is capable of binding cytokines such as TNFα and IL-1β through fibronectin (*60*), and these cytokines sequestered within the IVD matrix may continue stimulating an IVDD response on affected cells. The relatively higher cell proliferation rate of calls cultured in Basal media suggests that cells removed from the matrix have the capacity to restore some of their

proliferative capabilities. This finding therefore shows that it may be possible to rescue degenerative cells by modulating its microenvironment. It also suggests that autologous cell therapy using culture expanded AF cells may be a feasible option if these cells can be delivered in a way that protects these cells from the cytokines in the matrix. However, cell therapies for IVD repair are challenging because autologous cells may be more susceptible to microenvironmental stress and die after re-injection, and if they survive would compete with resident IVD cells in the limited nutrient environment of the IVD (*49, 61*). Therefore, consideration of biomaterials or engineered constructs such as recently developed bioactive tension-activated nanofiber patches that can modulate pro-inflammatory responses through IL1-β pathway may be required (*62*).Those approaches can also target TNFR1 or otherwise protect delivered and native IVD cells from the complex pro-inflammatory environment of the IVD.

This study characterized TNFR-specific responses in IVDD. Blocking TNFR1 but not TNFR2 restored some metabolic activities and cell proliferation. Supporting the importance of TNFR1 in IVDD, in a recent rat model CRISPR modulated cells with inhibited TNFR1 showed improved IVD regeneration and pain response (*63*). Interestingly, a reduced pain-like behaviors was found in vivo while our data suggests a depletion of axonogenesis and presynaptic endocytosis when blocking the TNFR1 pathway, which seem to underline the critical role of TNFR1 signaling in pain response and the potential of TNFR1 as target for anti-pain treatments. Blocking TNFR1 in this study enriched GO terms related to inflammatory responses, which is likely driven by the complex mixture of cytokines remaining within the CM in addition to TNFα. The more robust inflammatory response with TNFR1 inhibition may be a key piece of shifting the chronic ‘frustrated healing’ states in IVDD to a more reparative healing response since regenerative healing in tendons requires a more robust and short-term immune response compared to inferior

adult healing (*64, 65*). Macrophages and the timing of their recruitment also seem to be critical for successful tissue regeneration, which has been shown in skin repair whereby early-, mid-, and late-stage macrophage depletion inhibited normal scarring, reduced vessel formation, and altered the pattern of scar formation, respectively (*66*). Furthermore, acute inflammatory responses have been suggested to protect against the development of chronic pain, suggesting benefits for a more robust inflammatory response (*67*). Inflammatory responses for tissue regeneration are known to be dependent on species, tissue, timing, and age, which will determine the cells involved in the healing process (*68*). Therefore, the enhanced inflammatory response found in this study with TNFR1 inhibition is likely to be an effort to recruit non-IVD cells and mount a reparative response. The increased immune response is highly provocative when we consider the IVD regeneration literature has a substantial focus on the balance of anabolic vs. catabolic responses and inhibition of the pro-inflammatory responses (*9, 49*). We speculate that rescue of the hAF cell proliferation and cell cycle responses is likely to be a more important therapeutic target than suppression of the inflammatory response, and this hypothesis needs further investigation.

Modulation of TNFR2 had no effect on hAF cells, which we suspect was related to the lack of TNFR2 signaling in native IVD cells. The limited TNFR2 expression in IVD cells found in this study was a strong finding identified using scRNA-seq and IHC methods and blocking studies. Lack of TNFR2 in IVD cells has potential for a paradigm shift suggesting IVD cells do not have the epigenetic programs to shift towards a repair/regeneration response and challenging the concept that the harsh IVD nutritional microenvironment is the main (or only) limitation in poor IVD healing. Nevertheless, Wang et al., found an increase of IVD degeneration in TNFR2$^{-/-}$ mice with greater IVD degeneration score, and decreased IVD height and MRI signal (*37*). TNFR2 is expressed in only a few cell types, including dendritic cells, macrophages and T cells (*69*). Our

study together with the literature therefore suggests that TNFR2 dependent healing identified by Wang et al., is likely to involve macrophages and other TNFR2 expressing cells more than native IVD cells which express little TNFR2. Wang et al., further showed that Atsttrin significantly improved IVD degeneration score and MRI signaling in TNFR1$^{-/-}$ mice, whereas TNFR2$^{-/-}$ mice were not affected, suggesting Atsttrin was primarily TNFR2-dependent. Therefore, we attribute the lack of Atsttrin effects in our study to the lack of TNFR2 in IVD cells. OA studies also showed increased healing when using Atsttrin in a mouse in vivo model with lower OA degeneration scores and increased matrix deposition (*35, 36, 70*). This study in the context of the literature suggests that TNFR1 signaling by IVD cells may be important in recruiting TNFR2 expressing cells (e.g., inflammatory cells) that play roles promoting IVD healing.

This study provides important insights into cytokines and cells in IVDD and herniation pathophysiology and identified TNFR1 and not TNFR2 modulation as important therapeutic targets, yet some limitations and future studies need to be considered. We are confident in the finding that these cytokines identified in IVDD CM are produced at substantially greater levels in macrophages than IVD cells, yet the particularly small number of macrophages detected produced, and origin of the high cytokine protein levels needs further analyses and consideration. The particularly small number of macrophages detected during scRNA-seq analyses may result from selective loss of macrophages during the overnight IVD cell isolation. We made substantial efforts to shorten our IVD cell isolation procedures for scRNA-seq analyses, yet found very low IVD cell yields and poor cell quality with shorter digestion periods. Therefore, overnight digestion of IVD tissue was required to release sufficient numbers of high quality IVD cells from the dense extracellular matrix for the analyses. The scRNA-seq analyses were performed at a single time point, and it is possible that the IVD cells at different stages of IVD injury and degeneration could

express multiple cytokines at higher levels. Future animal studies assessing IVDs at multiple time points after injuries, and comparisons of sequencing signatures between bulk vs scRNA-seq may help elucidate if the macrophages of IVD cells or a combination are the main source of these cytokines found in IVDD tissues. The hAF cell in vitro model is capable as a screening tool for a variety of potential drugs focused on IVD cell therapies and identified potential roles in axonogenesis and presynaptic endocytosis, however, investigating the interplay between IVD and nerve cells to predict pain responses requires more complex model systems than hAF cells in 2D culture. The cytokines released from IVDD tissues with herniation were compared to Basal and was appropriate for screening effects of TNFR1 and TNFR2 blocking. Future investigations using CM from healthy IVD samples would provide a useful control for larger therapy screening studies, yet were not used here because healthy IVD controls are not available from surgical subjects (and since cells isolated from healthy IVD autopsy samples are not directly comparable to cells isolated from surgical tissue). IVDD samples in this study were obtained from herniated samples and may involve a more pro-inflammatory response than IVDD specimens without herniation and is an important consideration while interpreting these results, although we highlight the high relevance of these human subject specimens from clinical back pain patients.

In conclusion, this study demonstrated that IVDD tissue with herniation contains a complex collection of many pro- and anti-inflammatory cytokines, that are predominantly expressed by M1 type macrophage derived cells. The largest effects of IVDD CM were to inhibit the hAF cell metabolic response and stimulate senescence, suggesting IVD cell cycle and metabolic rate responses may be more important rescue parameters than relative anabolic and catabolic responses. Targeted TNFR1 blocking had potential to reactivate hAF cell proliferative capacities in order to enable them to mount a more robust inflammatory response, which is likely to be important for

healing and recruitment of inflammatory cells. The highly limited TNFR2 expression in native IVD cells provides a novel theory that frustrated healing in IVDD is partly related to IVD cells lacking the epigenetic 'architecture' to shift to a pro-reparative response under cytokine challenges and must instead rely on recruiting TNFR2 expressing cells, such as macrophages for repair responses. Future therapeutic strategies for IVDD with herniation, therefore, may consider TNFR1 inhibition to resume IVD cell cycle in combination with recruitment or delivery of TNFR2 expressing cells that may offer additional benefit to address for more complete IVD repair.

MATERIALS AND METHODS

Tissue source

This study was approved by Mount Sinai Institutional Review Board (IRB# STUDY-19-01394-MOD001) project titled 'Orthopedic Cell and Tissue Repository'. For media conditioning, nine human IVDs were obtained from patients (6 males, 3 females), 34-65 years old (mean = 50.4). For cell isolation, six IVDs were obtained (4 males, 2 females), 25-71 years old (mean = 45.8). The collected specimen was assessed, and AF and NP were carefully separated for cell isolation. All patients experienced back or neck pain and underwent disc fusion or discectomy surgery. Assessment of the disease state was performed using Pfirrmann grading on Pre-surgery MRI images. Informed consent from patients was given prior to surgery Specimen information is given in table S1. Human samples for IHC were obtained from an institutional biobank of cadaveric IVDs. This study included 15 lumbar IVDs (8 Male, 7 Female) (table S3). The morphological degeneration of each sample was quantified using the Rutgers degeneration scale that ranges from grade 1-12, with 12 as the most degenerated (*71*). Each sample was graded for Rutgers grade by

three trained and independent graders who were blinded to the sample age, sex, and to the Pfirrman grade.

Conditioning of media

Immediately after IVD collection, tissues were cut into smaller pieces, if necessary and washed three times in Phosphate-Buffered Saline (PBS) supplemented with 2% Penicillin / Streptomicin (10,000 U/mL, Gibco) and Primocin (100 µg/mL, Invivogen). Afterwards, the tissue was cultured in 10 mL media (RoosterNourish™-MSC, RoosterBio) per gram tissue and maintained under constant agitation at 37°C and 5% CO_2 for 72 hours. ADF -CM was collected and frozen as individual samples at -80°C for later analysis. After initial characterization and analysis of statistical differences between samples, media collected from 9 individuals were combined to reduce number of variables in consecutive experiments.

Media analysis/ Multiplex cytokine array analysis

For quantification of pro-inflammatory cytokines released from surgical samples, media was sampled and analyzed using a Human Cytokine/Chemokine 48-Plex Discovery Assay® Array (catalog no. HD48, Eve Technologies). The 48-Plex Discovery Assay used 100 µL of undiluted cell culture media per run and each run was performed in duplicates. Fluorescence intensity values were derived from the discovery assay and are in direct proportion to the concentration of proteins in the samples.

hAF cell isolation and culture

The hAF cells were isolated from surgical specimens. Briefly, collected AF tissue was finely minced and digested using collagenase type I (400 U/mL, Gibco, USA) for 12 hours under constant agitation at 37°C in serum-free hg-DMEM containing Penicillin / Streptomicin and Amphotericin

B (0.25 µg/mL). Using a 70 µm cell strainer debris was removed from the tissue/cell suspension. Cells were either immediately processed for scRNA-seq analysis or seeded at 5,000 cells/cm^2 in RoosterNourish™-MSC media (Rooster Bio) under normoxic (21% O_2) conditions at 37°C and 5 % CO_2.

scRNAseq

Immediately after isolation, cells of from 3 patients (5 specimens) were further cleaned up using the LeviCell system (Levitas Bio) according to manufacturer's protocols to remove excess debris. Afterwards, samples were processed according to Chromium 3' Gene Expression V3.1 Kit (10X Genomics, Pleasanton, CA) using manufacturer's guidelines. An estimated 5,000 cells were loaded onto each channel with a targeted cell recovery of approximately 3,000 cells/sample. This was followed by sequencing on a S4 NovaSeq chip (Illumina Inc., San Diego, CA). Qubit 3 (Fisher Scientific) and 2100 Bioanalyzer (Agilent Technologies, Santa Clara, CA) were used for quality check of library.

scRNAseq analysis

Sequencing data were aligned and quantified using the Cell Ranger Single-Cell Software Suite (version 7.1.0, 10x Genomics) against the reference genome GRCh38. The pipeline grouped and de-duplicated reads confidently mapped to the transcriptome by 10X cellular barcodes and UMIs (Unique Molecular Identifiers), then summarized counts into feature-barcode matrices. The R-based package Seurat (v4.3) was used for further processing and analysis (*72*). For quality control, standard pre-processing steps were applied to remove cells with <500 mapped genes, <1,000 gene counts, and >20% mitochondrial content. The data were further filtered to removed genes detected in less than 5% of cells per sample. All pre-processed samples were RPCA-integrated using the SCTransform normalization method. The top 4,000 variable features were used to define 20

integration anchors. PCA identified 30 dimensions for unsupervised graph-based clustering via uniform manifold approximation and projection (UMAP) at a 0.5 resolution parameter (*73*). Genes expressed in >10% of cells in a cluster with an average $\log_2$-fold change >0.25 were selected as DEGs using FindMarkers. Cell types identified from the resulting UMAP were manually annotated based on each cluster's DEG profile and further confirmed using UniCell, an unbiased cell type deconvolution pipeline that leverages a deep learning neural network pre-trained on >28 million annotated single cells from published studies *(43)*. Pathway enrichment was performed using Enrichr to determine significantly enriched biological pathways based on upregulated DEGs, and normalized enrichment scores were reported for top gene pathway sets.

Cell culture conditions for individual experiments

When primary cells reach 80-85 % confluency, media was changed according to study design (Table 1). Specifically, for Basal group, media was replaced by fresh RoosterNourish™-MSC media (Rooster Bio), for the dosing experiment, CM was diluted using Basal media and for the TNFR blocking experiment, CM was supplemented with anti-TNFR1 (10 µg/mL, MAB225-500, R&D Systems), anti-TNFR2 (10 µg/mL, MAB726-500, R&D Systems) or Atsttrin (200 ng/mL, manufactured in-house). Cultures were moved into a hypoxic environment (5% O_2) for the duration of the experiment.

MTT assay

To determine the metabolic activity and respective cell viability, cells were cultured in media, supplemented with 0.5 mg/mL 3-[4,5-dimethylthiazol-2-yl]-2,5-diphenyltetrazolium bromide (MTT, Sigma, USA) for 4 hrs at 37ºC. Afterwards, cells were lysed using Dimethyl Sulfoxide to release insoluble formazan, which was quantified at λ_{ab} = 540 nm with λ_{ref} >650 nm. Absorbance was normalized to basal group to compare between replicates.

Gene expression analysis using qRT-PCR

Quantitative reverse transcription polymerase chain reaction (qRT-PCR) was used to quantify the gene expression of hAF cells that were retained during in vitro culture of CM model optimization. RNA was extracted from samples using the RNeasy Micro Kit (QIAGEN INC, USA) according to manufacturer instructions and eluted in 15 µL RNase free water. RNA concentration was quantified using a Thermo Scientific NanoDrop™ One UV–Vis spectrophotometer (Thermo Fisher Scientific) followed by synthesis of complementary DNA (cDNA) using the SuperScript® VILO™ MasterMix (Invitrogen, Waltham, MA) according to manufacturer instructions. The PowerUp™ SYBR™ Green Master Mix (Invitrogen) was used with human primers for Glyceraldehyde 3-Phosphate Dehydrogenase (GAPDH, Hs.PT.39a.22214836), TNF Receptor Superfamily Member 1A (TNFRSF1A, Hs.PT.58.19429998) and TNF Receptor Superfamily Member 1B (TNFRSF1B, Hs.PT.58.40638488) (all from Integrated DNA Technologies, Coralville IA) according to manufacturer instructions for qRT-PCR. qRT-PCR was performed by the Mount Sinai qPCR CoRE using an ABI PRISM 7900HT sequence detection system with robotic arms (Applied Biosystems, Foster City, CA). Data was analyzed using the $2^{-\Delta\Delta Ct}$ method (*74*), normalized to housekeeping gene glyceraldehyde 3-phosphate dehydrogenase (GAPDH) and relative to hAF cells cultured basal media. $2^{-\Delta\Delta Ct}$ calculations were conducted using Microsoft Excel (Microsoft, Redmond, NM).

Bulk RNA sequencing

Bulk RNAseq was used to evaluate changes in gene expression of hAF cells after TNFα signaling modulation ("TNFR blocking"). RNA was extracted from samples using the RNeasy Micro Kit (QIAGEN INC, USA) according to manufacturer instructions with DNase application and eluted in 15 µL RNase free water. RNA concentration was quantified using a Thermo Scientific

NanoDrop™ One UV–Vis spectrophotometer (Thermo Fisher Scientific). RNA integrity (RIN) was measured with an Agilent 2100 BioAnalyzer. 2 μg of total RNA from each sample were used for library preparation. Each library was constructed from RNA from hAF cells from 5 individual donors. First, polyadenylated transcripts were enriched using NEXTFLEX Poly(a) Beads 2.0 (PerkinElmer); then, RNA libraries were prepared using the NEXTFLEX® Rapid Directional RNA-Seq Kit 2.0 (PerkinElmer). Library concentration was measure by Qubit, while library quality and size were calculated with an Agilent 2100 BioAnalyzer. Single-end read sequencing was performed using an Illumina NextSeq 550 instrument and a High-output kit, at a depth of 33 million reads per sample.

Differential expression of bulk transcriptomic analysis

FASTQ files of sequenced reads using the aforementioned bulk RNA sequencing data were aligned to human transcriptome (GENCODE annotation model p10 release 27) using the STAR aligner (v2.5.3a), with an average alignment rate of over 80%. Gene-level expression was quantified by the featureCounts (v1.6.3) and normalized by the voom function in R/limma packages. Differential expression was called by R/limma. PCA and clustering were performed in R. Significant DEGs were determined using R/limma at a false discovery rate of 5%, with a fold change greater than or equal to 2. Gene ontology and pathway enrichment was performed using Enrichr to determine significantly enriched or depleted pathways, and normalized enrichment scores reported for top gene ontology and pathway sets.

QIAGEN Ingenuity Pathway Analysis

The network analyses were generated through the use of QIAGEN IPA (QIAGEN Inc., https://digitalinsights.qiagen.com/IPA) using their developed algorithms (*75*). Included were DEGs with a FC <-1.5 and >1.5 and a p-value ≤0.01.

SA-β-Gal staining and quantification

Staining was performed using the Senescence Detection Kit (Abcam, ab65351) following the manufacturer's protocol. Briefly, hAF cells were fixed for 15 min with 1× fixation solution, washed with PBS and incubated overnight at 37 °C in 1× staining solution. Brightfield images were captured at 20X on the VWR® Trinocular Inverted Microscope. SA-β-Gal positive cells from 5 biological replicates with n=9 technical replicates per group were analyzed using the ImageJ Cell Counter Plugin.

Cleaved-Casp3 staining and analysis

hAF cells were fixed in Z-fix formalin fixative for 10 min at room temperature followed by permeabilization for permeabilization using 0.5% TritonX-100 for 5 minutes. Cells were incubated for 1 hour at room temperature with serum-free protein block (Dako X0909) to block non-specific binding sites followed by Cleaved-Casp3 primary antibody (Abcam, ab49822, 1:1000) at 4°C over night. Next, the secondary antibody (Cy™5 Donkey Anti-Rabbit IgG, 1:400) (Jackson ImmunoResearch, 711-175-152) was added for 1 hour. Finally sections were cover slipped using ProLong™ Gold antifade reagent with DAPI (Invitrogen P36931). Dual-channel images were captured at 20X on the Zeiss AxioImager fluorescence microscope. For Co-localization analysis, ImageJ Plugin "EzColocalization" was used to quantify Pearson's correlation coefficient (*76*). For nuclear fluorescent intensity, the Intensity Density (IntDen) of Casp3 signal within the nuclear reason was determined using ImageJ. A total of 5 biological replicates with n=4 technical replicates were analyzed.

IHC analysis of human IVDs

Human specimens were fixed in formaldehyde, embedded in resin, and sectioned in the sagittal plane as previously described (*77*). Mid-sagittal 5°µm sections from each sample were stained with picrosirius red/alcian blue (PR/AB) for morphological reference. Prior to staining, tissue sections were deplasticized and rehydrated. Sections were then treated with proteinase K (S3020, Dako North America, Carpinteria, CA) followed by protein block (X0909, Dako North America). At room temperature, sections were incubated for one hour with either rabbit polyclonal primary antibody against TNF Receptor 1 (dilution 1:400, ab111119, Abcam, Cambridge, MA), recombinant rabbit monoclonal primary antibody against TNF Receptor 2 [EPR1653] (dilution 1:200, ab109322, Abcam, Cambridge, MA) or normal rabbit serum (ab7487, Abcam) as a negative control. Then sections were incubated for 30 minutes at room temperature with anti-rabbit IgG peroxidase secondary antibodies (ImmPRESS reagent, Vector Laboratories, Burlingame, CA). Afterwards the sections were treated with hydrogen peroxide block (ab94710, Abcam) for 10 min followed by diaminobenzidine-based peroxidase substrate for a minute (ImmPACT DAB Vector Laboratories). Finally, the sections were counterstained with 0.1% toluidine blue before mounting. Whole digital slide images were obtained using NanoZoomer S210 from Hamamatsu. Quantification of TNFR1/2 was performed using HALO Image Analysis Platform (v3.6.4134.137, Indica Labs, Albuquerque, NM, USA). Briefly, tissues were annotated to identify the regions to include in the analysis. Once the analysis area is defined, TNFR1/2 is quantified using HALO Multiplex module. The bright filed algorithm uses color deconvolution to separate the chromogenic stains and this allows for the generation of the "markup" image of the of the separated chromogenic stains based on selected settings that will generate the results.

Statistical analysis

The statistical analyses were performed in R (v4.2.3) using R-based package Seurat (v4.3) for analysis of scRNA-seq data and R-based Limma for analysis of bulk RNA-seq data. For all other data, statistical analyses were performed using GraphPad Prism (v10) software. One-way ANOVA or Two-way ANOVA with Tukey's post-tests were used to compare between groups. Results were displayed as mean ± standard deviation. Significance was accepted at a level of $p < 0.05$.

References:

1. J. Hartvigsen, M. J. Hancock, A. Kongsted, Q. Louw, M. L. Ferreira, S. Genevay, D. Hoy, J. Karppinen, G. Pransky, J. Sieper, R. J. Smeets, M. Underwood, G. Lancet Low Back Pain Series Working, What low back pain is and why we need to pay attention. *Lancet*, (2018); published online EpubMar 20 (10.1016/S0140-6736(18)30480-X).
2. D. Hoy, C. Bain, G. Williams, L. March, P. Brooks, F. Blyth, A. Woolf, T. Vos, R. Buchbinder, A systematic review of the global prevalence of low back pain. *Arthritis Rheum* **64**, 2028-2037 (2012); published online EpubJun (10.1002/art.34347).
3. D. Hoy, L. March, P. Brooks, F. Blyth, A. Woolf, C. Bain, G. Williams, E. Smith, T. Vos, J. Barendregt, C. Murray, R. Burstein, R. Buchbinder, The global burden of low back pain: estimates from the Global Burden of Disease 2010 study. *Ann Rheum Dis* **73**, 968-974 (2014); published online EpubJun (10.1136/annrheumdis-2013-204428).
4. J. N. Katz, Lumbar disc disorders and low-back pain: socioeconomic factors and consequences. *J Bone Joint Surg Am* **88 Suppl 2**, 21-24 (2006); published online EpubApr (
5. K. Fujii, A. Lai, N. Korda, W. W. Hom, T. W. Evashwick-Rogler, P. Nasser, A. C. Hecht, J. C. Iatridis, Ex-vivo biomechanics of repaired rat intervertebral discs using genipin crosslinked fibrin adhesive hydrogel. *J Biomech* **113**, 110100 (2020); published online EpubDec 2 (10.1016/j.jbiomech.2020.110100).
6. J. C. Iatridis, S. B. Nicoll, A. J. Michalek, B. A. Walter, M. S. Gupta, Role of biomechanics on intervertebral disc degeneration and regenerative therapies: What needs repairing in the IVD and what are promising biomaterials for its repair? *The Spine Journal*, In Press (2012).
7. H. E. Jacobsen, A. N. Khan, M. E. Levine, C. G. Filippi, N. O. Chahine, Severity of intervertebral disc herniation regulates cytokine and chemokine levels in patients with chronic radicular back pain. *Osteoarthritis Cartilage* **28**, 1341-1350 (2020); published online EpubOct (10.1016/j.joca.2020.06.009).
8. C. L. Le Maitre, A. J. Freemont, J. A. Hoyland, The role of interleukin-1 in the pathogenesis of human intervertebral disc degeneration. *Arthritis Res Ther* **7**, R732-745 (2005).
9. M. V. Risbud, I. M. Shapiro, Role of cytokines in intervertebral disc degeneration: pain and disc content. *Nat Rev Rheumatol* **10**, 44-56 (2014); published online EpubJan (10.1038/nrrheum.2013.160).
10. A. Lai, A. Moon, D. Purmessur, B. Skovrlj, D. M. Laudier, B. A. Winkelstein, S. K. Cho, A. C. Hecht, J. C. Iatridis, Annular puncture with tumor necrosis factor-alpha injection enhances painful behavior with disc degeneration in vivo. *Spine J* **16**, 420-431 (2016); published online EpubMar (10.1016/j.spinee.2015.11.019).
11. B. A. Walter, D. Purmessur, M. Likhitpanichkul, A. Weinberg, S. K. Cho, S. A. Qureshi, A. C. Hecht, J. C. Iatridis, Inflammatory Kinetics and Efficacy of Anti-inflammatory Treatments on Human Nucleus Pulposus Cells. *Spine (Phila Pa 1976)* **40**, 955-963 (2015); published online EpubJul 1 (10.1097/BRS.0000000000000932).
12. D. Purmessur, A. J. Freemont, J. A. Hoyland, Expression and regulation of neurotrophins in the nondegenerate and degenerate human intervertebral disc. *Arthritis Res Ther* **10**, R99 (2008)10.1186/ar2487

ar2487 [pii]).

13. S. M. Richardson, D. Purmessur, P. Baird, B. Probyn, A. J. Freemont, J. A. Hoyland, Degenerate human nucleus pulposus cells promote neurite outgrowth in neural cells. *PLoS One* **7**, e47735 (2012)10.1371/journal.pone.0047735).
14. W. Jiang, J. D. Glaeser, G. Kaneda, J. Sheyn, J. T. Wechsler, S. Stephan, K. Salehi, J. L. Chan, W. Tawackoli, P. Avalos, C. Johnson, C. Castaneda, L. E. A. Kanim, T. Tanasansomboon, J. E. Burda, O. Shelest, H. Yameen, T. G. Perry, M. Kropf, J. M. Cuellar, D. Seliktar, H. W. Bae, L. S. Stone, D. Sheyn, Intervertebral disc human nucleus pulposus cells associated with back pain trigger neurite outgrowth in vitro and pain behaviors in rats. *Sci Transl Med* **15**, eadg7020 (2023); published online EpubDec 6 (10.1126/scitranslmed.adg7020).
15. J. Koroth, E. O. Buko, R. Abbott, C. P. Johnson, B. M. Ogle, L. S. Stone, A. M. Ellingson, E. W. Bradley, Macrophages and Intervertebral Disc Degeneration. *Int J Mol Sci* **24**, (2023); published online EpubJan 10 (10.3390/ijms24021367).
16. B. A. Walter, M. Likhitpanichkul, S. Illien-Junger, P. J. Roughley, A. C. Hecht, J. C. Iatridis, TNFalpha transport induced by dynamic loading alters biomechanics of intact intervertebral discs. *PLoS One* **10**, e0118358 (2015)10.1371/journal.pone.0118358).
17. C. Wang, X. Yu, Y. Yan, W. Yang, S. Zhang, Y. Xiang, J. Zhang, W. Wang, Tumor necrosis factor-alpha: a key contributor to intervertebral disc degeneration. *Acta Biochim Biophys Sin (Shanghai)* **49**, 1-13 (2017); published online EpubJan (10.1093/abbs/gmw112).
18. R. A. Autio, J. Karppinen, J. Niinimaki, R. Ojala, N. Veeger, T. Korhonen, H. Hurri, O. Tervonen, The effect of infliximab, a monoclonal antibody against TNF-alpha, on disc herniation resorption: a randomized controlled study. *Spine (Phila Pa 1976)* **31**, 2641-2645 (2006); published online EpubNov 1 (10.1097/01.brs.0000244616.64962.9e).
19. T. Korhonen, J. Karppinen, L. Paimela, A. Malmivaara, K. A. Lindgren, C. Bowman, A. Hammond, B. Kirkham, S. Jarvinen, J. Niinimaki, N. Veeger, M. Haapea, M. Torkki, O. Tervonen, S. Seitsalo, H. Hurri, The treatment of disc-herniation-induced sciatica with infliximab: one-year follow-up results of FIRST II, a randomized controlled trial. *Spine (Phila Pa 1976)* **31**, 2759-2766 (2006); published online EpubNov 15 (10.1097/01.brs.0000245873.23876.1e).
20. S. P. Cohen, N. Bogduk, A. Dragovich, C. C. Buckenmaier, 3rd, S. Griffith, C. Kurihara, J. Raymond, P. J. Richter, N. Williams, T. L. Yaksh, Randomized, double-blind, placebo-controlled, dose-response, and preclinical safety study of transforaminal epidural etanercept for the treatment of sciatica. *Anesthesiology* **110**, 1116-1126 (2009); published online EpubMay (10.1097/ALN.0b013e3181a05aa0).
21. T. Sainoh, S. Orita, M. Miyagi, G. Inoue, H. Kamoda, T. Ishikawa, K. Yamauchi, M. Suzuki, Y. Sakuma, G. Kubota, Y. Oikawa, K. Inage, J. Sato, Y. Nakata, J. Nakamura, Y. Aoki, T. Toyone, K. Takahashi, S. Ohtori, Single Intradiscal Administration of the Tumor Necrosis Factor-Alpha Inhibitor, Etanercept, for Patients with Discogenic Low Back Pain. *Pain Med* **17**, 40-45 (2016); published online EpubJan (10.1111/pme.12892).
22. S. Genevay, S. Viatte, A. Finckh, P. Zufferey, F. Balague, C. Gabay, Adalimumab in severe and acute sciatica: a multicenter, randomized, double-blind, placebo-controlled trial. *Arthritis Rheum* **62**, 2339-2346 (2010); published online EpubAug (10.1002/art.27499).

23. P. Goupille, D. Mulleman, G. Paintaud, H. Watier, J. P. Valat, Can sciatica induced by disc herniation be treated with tumor necrosis factor alpha blockade? *Arthritis Rheum* **56**, 3887-3895 (2007); published online EpubDec (10.1002/art.23051).
24. S. Jing, C. Yang, X. Zhang, S. Wen, Y. Li, Efficacy and safety of etanercept in the treatment of sciatica: A systematic review and meta-analysis. *J Clin Neurosci* **44**, 69-74 (2017); published online EpubOct (10.1016/j.jocn.2017.06.054).
25. B. J. Freeman, G. L. Ludbrook, S. Hall, M. Cousins, B. Mitchell, M. Jaros, M. Wyand, J. R. Gorman, Randomized, double-blind, placebo-controlled, trial of transforaminal epidural etanercept for the treatment of symptomatic lumbar disc herniation. *Spine (Phila Pa 1976)* **38**, 1986-1994 (2013); published online EpubNov 1 (10.1097/01.brs.0000435140.61593.4c).
26. T. W. Evashwick-Rogler, A. Lai, H. Watanabe, J. M. Salandra, B. A. Winkelstein, S. K. Cho, A. C. Hecht, J. C. Iatridis, Inhibiting tumor necrosis factor-alpha at time of induced intervertebral disc injury limits long-term pain and degeneration in a rat model. *JOR Spine* **1**, (2018); published online EpubJun (10.1002/jsp2.1014).
27. P. Andrade, V. Visser-Vandewalle, M. Philippens, M. A. Daemen, H. W. Steinbusch, W. A. Buurman, G. Hoogland, Tumor necrosis factor-alpha levels correlate with postoperative pain severity in lumbar disc hernia patients: opposite clinical effects between tumor necrosis factor receptor 1 and 2. *Pain* **152**, 2645-2652 (2011); published online EpubNov (10.1016/j.pain.2011.08.012).
28. G. D. Kalliolias, L. B. Ivashkiv, TNF biology, pathogenic mechanisms and emerging therapeutic strategies. *Nat Rev Rheumatol* **12**, 49-62 (2016); published online EpubJan (10.1038/nrrheum.2015.169).
29. J. Huang, S. Yu, C. Ji, J. Li, Structural basis of cell apoptosis and necrosis in TNFR signaling. *Apoptosis* **20**, 210-215 (2015); published online EpubFeb (10.1007/s10495-014-1061-5).
30. S. Yang, J. Wang, D. D. Brand, S. G. Zheng, Role of TNF-TNF Receptor 2 Signal in Regulatory T Cells and Its Therapeutic Implications. *Front Immunol* **9**, 784 (2018)10.3389/fimmu.2018.00784).
31. L. M. Sedger, M. F. McDermott, TNF and TNF-receptors: From mediators of cell death and inflammation to therapeutic giants - past, present and future. *Cytokine Growth Factor Rev* **25**, 453-472 (2014); published online EpubAug (10.1016/j.cytogfr.2014.07.016).
32. A. Rajput, C. F. Ware, in *Encyclopedia of Cell Biology*, A. B. Ralph, D. S. Philip, Eds. (Academic Press, Waltham, 2016), pp. 354-363.
33. C. J. Liu, X. Bosch, Progranulin: a growth factor, a novel TNFR ligand and a drug target. *Pharmacol Ther* **133**, 124-132 (2012); published online EpubJan (10.1016/j.pharmthera.2011.10.003).
34. W. Tang, Y. Lu, Q. Y. Tian, Y. Zhang, F. J. Guo, G. Y. Liu, N. M. Syed, Y. Lai, E. A. Lin, L. Kong, J. Su, F. Yin, A. H. Ding, A. Zanin-Zhorov, M. L. Dustin, J. Tao, J. Craft, Z. Yin, J. Q. Feng, S. B. Abramson, X. P. Yu, C. J. Liu, The growth factor progranulin binds to TNF receptors and is therapeutic against inflammatory arthritis in mice. *Science* **332**, 478-484 (2011); published online EpubApr 22 (10.1126/science.1199214).
35. Y. P. Zhao, B. Liu, Q. Y. Tian, J. L. Wei, B. Richbourgh, C. J. Liu, Progranulin protects against osteoarthritis through interacting with TNF-alpha and beta-Catenin signalling. *Ann Rheum Dis* **74**, 2244-2253 (2015); published online EpubDec (10.1136/annrheumdis-2014-205779).

36. J. L. Wei, W. Fu, Y. J. Ding, A. Hettinghouse, M. Lendhey, R. Schwarzkopf, O. D. Kennedy, C. J. Liu, Progranulin derivative Atsttrin protects against early osteoarthritis in mouse and rat models. *Arthritis Res Ther* **19**, 280 (2017); published online EpubDec 19 (10.1186/s13075-017-1485-8).
37. S. Wang, G. Sun, P. Fan, L. Huang, Y. Chen, C. Chen, Distinctive roles of tumor necrosis factor receptor type 1 and type 2 in a mouse disc degeneration model. *J Orthop Translat* **31**, 62-72 (2021); published online EpubNov (10.1016/j.jot.2021.11.003).
38. D. Purmessur, B. A. Walter, P. J. Roughley, D. M. Laudier, A. C. Hecht, J. Iatridis, A role for TNFalpha in intervertebral disc degeneration: a non-recoverable catabolic shift. *Biochem Biophys Res Commun* **433**, 151-156 (2013); published online EpubMar 29 (10.1016/j.bbrc.2013.02.034).
39. R. Maidhof, T. Jacobsen, A. Papatheodorou, N. O. Chahine, Inflammation induces irreversible biophysical changes in isolated nucleus pulposus cells. *PLoS One* **9**, e99621 (2014)10.1371/journal.pone.0099621).
40. X. Wang, H. Wang, H. Yang, J. Li, Q. Cai, I. M. Shapiro, M. V. Risbud, Tumor necrosis factor-alpha- and interleukin-1beta-dependent matrix metalloproteinase-3 expression in nucleus pulposus cells requires cooperative signaling via syndecan 4 and mitogen-activated protein kinase-NF-kappaB axis: implications in inflammatory disc disease. *Am J Pathol* **184**, 2560-2572 (2014); published online EpubSep (10.1016/j.ajpath.2014.06.006).
41. Z. I. Johnson, A. C. Doolittle, J. W. Snuggs, I. M. Shapiro, C. L. Le Maitre, M. V. Risbud, TNF-alpha promotes nuclear enrichment of the transcription factor TonEBP/NFAT5 to selectively control inflammatory but not osmoregulatory responses in nucleus pulposus cells. *J Biol Chem* **292**, 17561-17575 (2017); published online EpubOct 20 (10.1074/jbc.M117.790378).
42. H. Ding, J. Wei, Y. Zhao, Y. Liu, L. Liu, L. Cheng, Progranulin derived engineered protein Atsttrin suppresses TNF-alpha-mediated inflammation in intervertebral disc degenerative disease. *Oncotarget* **8**, 109692-109702 (2017); published online EpubDec 12 (10.18632/oncotarget.22766).
43. D. Charytonowicz, R. Brody, R. Sebra, Interpretable and context-free deconvolution of multi-scale whole transcriptomic data with UniCell deconvolve. *Nat Commun* **14**, 1350 (2023); published online EpubMar 11 (10.1038/s41467-023-36961-8).
44. B. K. Tye, MCM proteins in DNA replication. *Annu Rev Biochem* **68**, 649-686 (1999)10.1146/annurev.biochem.68.1.649).
45. L. Han, Z. Chen, K. Yu, J. Yan, T. Li, X. Ba, W. Lin, Y. Huang, P. Shen, Y. Huang, K. Qin, Y. Geng, Y. Liu, Y. Wang, S. Tu, Interleukin 27 Signaling in Rheumatoid Arthritis Patients: Good or Evil? *Front Immunol* **12**, 787252 (2021)10.3389/fimmu.2021.787252).
46. M. L. Whitfield, G. Sherlock, A. J. Saldanha, J. I. Murray, C. A. Ball, K. E. Alexander, J. C. Matese, C. M. Perou, M. M. Hurt, P. O. Brown, D. Botstein, Identification of genes periodically expressed in the human cell cycle and their expression in tumors. *Mol Biol Cell* **13**, 1977-2000 (2002); published online EpubJun (10.1091/mbc.02-02-0030).
47. A. Riba, A. Oravecz, M. Durik, S. Jimenez, V. Alunni, M. Cerciat, M. Jung, C. Keime, W. M. Keyes, N. Molina, Cell cycle gene regulation dynamics revealed by RNA velocity and deep-learning. *Nat Commun* **13**, 2865 (2022); published online EpubMay 23 (10.1038/s41467-022-30545-8).

48. K. T. Weber, D. O. Alipui, C. P. Sison, O. Bloom, S. Quraishi, M. C. Overby, M. Levine, N. O. Chahine, Serum levels of the proinflammatory cytokine interleukin-6 vary based on diagnoses in individuals with lumbar intervertebral disc diseases. *Arthritis Res Ther* **18**, 3 (2016); published online EpubJan 7 (10.1186/s13075-015-0887-8).
49. Y. C. Huang, J. P. Urban, K. D. Luk, Intervertebral disc regeneration: do nutrients lead the way? *Nat Rev Rheumatol* **10**, 561-566 (2014); published online EpubSep (10.1038/nrrheum.2014.91).
50. M. A. Adams, P. Lama, U. Zehra, P. Dolan, Why do some intervertebral discs degenerate, when others (in the same spine) do not? *Clin Anat* **28**, 195-204 (2015); published online EpubMar (10.1002/ca.22404).
51. K. R. Nakazawa, B. A. Walter, D. M. Laudier, D. Krishnamoorthy, G. E. Mosley, K. L. Spiller, J. C. Iatridis, Accumulation and localization of macrophage phenotypes with human intervertebral disc degeneration. *Spine J* **18**, 343-356 (2018); published online EpubFeb (10.1016/j.spinee.2017.09.018).
52. C. L. Le Maitre, A. J. Freemont, J. A. Hoyland, Accelerated cellular senescence in degenerate intervertebral discs: a possible role in the pathogenesis of intervertebral disc degeneration. *Arthritis Res Ther* **9**, R45 (2007); published online EpubMay 11 (
53. A. Yee, M. P. Lam, V. Tam, W. C. Chan, I. K. Chu, K. S. Cheah, K. M. Cheung, D. Chan, Fibrotic-like changes in degenerate human intervertebral discs revealed by quantitative proteomic analysis. *Osteoarthritis Cartilage* **24**, 503-513 (2016); published online EpubMar (10.1016/j.joca.2015.09.020).
54. P. Patil, L. J. Niedernhofer, P. D. Robbins, J. Lee, G. Sowa, N. Vo, Cellular senescence in intervertebral disc aging and degeneration. *Curr Mol Biol Rep* **4**, 180-190 (2018); published online EpubDec (10.1007/s40610-018-0108-8).
55. T. Yurube, Y. Takeoka, Y. Kanda, R. Kuroda, K. Kakutani, Intervertebral disc cell fate during aging and degeneration: apoptosis, senescence, and autophagy. *N Am Spine Soc J* **14**, 100210 (2023); published online EpubJun (10.1016/j.xnsj.2023.100210).
56. E. Krock, D. H. Rosenzweig, A. J. Chabot-Dore, P. Jarzem, M. H. Weber, J. A. Ouellet, L. S. Stone, L. Haglund, Painful, degenerating intervertebral discs up-regulate neurite sprouting and CGRP through nociceptive factors. *J Cell Mol Med* **18**, 1213-1225 (2014); published online EpubJun (10.1111/jcmm.12268).
57. J. D. Stover, B. Lawrence, R. D. Bowles, Degenerative IVD conditioned media and acidic pH sensitize sensory neurons to cyclic tensile strain. *J Orthop Res* **39**, 1192-1203 (2021); published online EpubJun (10.1002/jor.24682).
58. S. Takeshita, K. Kaji, A. Kudo, Identification and characterization of the new osteoclast progenitor with macrophage phenotypes being able to differentiate into mature osteoclasts. *J Bone Miner Res* **15**, 1477-1488 (2000); published online EpubAug (10.1359/jbmr.2000.15.8.1477).
59. K. W. Kim, T. H. Lim, J. G. Kim, S. T. Jeong, K. Masuda, H. S. An, The origin of chondrocytes in the nucleus pulposus and histologic findings associated with the transition of a notochordal nucleus pulposus to a fibrocartilaginous nucleus pulposus in intact rabbit intervertebral discs. *Spine* **28**, 982-990 (2003); published online EpubMay 15 (
60. G. G. Vaday, R. Hershkoviz, M. A. Rahat, N. Lahat, L. Cahalon, O. Lider, Fibronectin-bound TNF-alpha stimulates monocyte matrix metalloproteinase-9 expression and regulates chemotaxis. *J Leukoc Biol* **68**, 737-747 (2000); published online EpubNov (

61. E. E. McDonnell, C. T. Buckley, Consolidating and re-evaluating the human disc nutrient microenvironment. *JOR Spine* **5**, e1192 (2022); published online EpubMar (10.1002/jsp2.1192).
62. A. P. Peredo, S. E. Gullbrand, C. S. Friday, B. S. Orozco, B. Dehghani, A. C. Jenk, E. D. Bonnevie, R. L. Hilliard, H. M. Zlotnick, G. R. Dodge, D. Lee, J. B. Engiles, M. W. Hast, T. P. Schaer, H. E. Smith, R. L. Mauck, Tension-activated nanofiber patches delivering an anti-inflammatory drug improve repair in a goat intervertebral disc herniation model. *Sci Transl Med* **15**, eadf1690 (2023); published online EpubNov 15 (10.1126/scitranslmed.adf1690).
63. J. D. Stover, M. A. R. Trone, J. Weston, C. Lewis, H. Levis, M. Philippi, M. Zeidan, B. Lawrence, R. D. Bowles, Therapeutic TNF-alpha Delivery After CRISPR Receptor Modulation in the Intervertebral Disc. *bioRxiv*, 2023.2005.2031.542947 (2023)10.1101/2023.05.31.542947).
64. B. Chazaud, Inflammation and Skeletal Muscle Regeneration: Leave It to the Macrophages! *Trends Immunol* **41**, 481-492 (2020); published online EpubJun (10.1016/j.it.2020.04.006).
65. K. L. Howell, D. A. Kaji, T. M. Li, A. Montero, K. Yeoh, P. Nasser, A. H. Huang, Macrophage depletion impairs neonatal tendon regeneration. *FASEB J* **35**, e21618 (2021); published online EpubJun (10.1096/fj.202100049R).
66. T. Lucas, A. Waisman, R. Ranjan, J. Roes, T. Krieg, W. Muller, A. Roers, S. A. Eming, Differential roles of macrophages in diverse phases of skin repair. *J Immunol* **184**, 3964-3977 (2010); published online EpubApr 1 (10.4049/jimmunol.0903356).
67. M. Parisien, L. V. Lima, C. Dagostino, N. El-Hachem, G. L. Drury, A. V. Grant, J. Huising, V. Verma, C. B. Meloto, J. R. Silva, G. G. S. Dutra, T. Markova, H. Dang, P. A. Tessier, G. D. Slade, A. G. Nackley, N. Ghasemlou, J. S. Mogil, M. Allegri, L. Diatchenko, Acute inflammatory response via neutrophil activation protects against the development of chronic pain. *Sci Transl Med* **14**, eabj9954 (2022); published online EpubMay 11 (10.1126/scitranslmed.abj9954).
68. S. A. Eming, T. A. Wynn, P. Martin, Inflammation and metabolism in tissue repair and regeneration. *Science* **356**, 1026-1030 (2017); published online EpubJun 9 (10.1126/science.aam7928).
69. O. Franzen, L. M. Gan, J. L. M. Bjorkegren, PanglaoDB: a web server for exploration of mouse and human single-cell RNA sequencing data. *Database (Oxford)* **2019**, (2019); published online EpubJan 1 (10.1093/database/baz046).
70. Q. Tian, Y. Zhao, J. J. Mundra, E. Gonzalez-Gugel, J. Jian, S. M. Uddin, C. Liu, Three TNFR-binding domains of PGRN act independently in inhibition of TNF-alpha binding and activity. *Front Biosci (Landmark Ed)* **19**, 1176-1185 (2014); published online EpubJun 1 (10.2741/4274).
71. J. P. Rutges, R. A. Duit, J. A. Kummer, J. E. Bekkers, F. C. Oner, R. M. Castelein, W. J. Dhert, L. B. Creemers, A validated new histological classification for intervertebral disc degeneration. *Osteoarthritis Cartilage* **21**, 2039-2047 (2013); published online EpubDec (10.1016/j.joca.2013.10.001).
72. R. Satija, J. A. Farrell, D. Gennert, A. F. Schier, A. Regev, Spatial reconstruction of single-cell gene expression data. *Nat Biotechnol* **33**, 495-502 (2015); published online EpubMay (10.1038/nbt.3192).

73. H. Shaath, R. Vishnubalaji, E. Elkord, N. M. Alajez, Single-Cell Transcriptome Analysis Highlights a Role for Neutrophils and Inflammatory Macrophages in the Pathogenesis of Severe COVID-19. *Cells* **9**, (2020); published online EpubOct 29 (10.3390/cells9112374).
74. K. J. Livak, T. D. Schmittgen, Analysis of relative gene expression data using real-time quantitative PCR and the 2(-Delta Delta C(T)) Method. *Methods* **25**, 402-408 (2001); published online EpubDec (
75. A. Kramer, J. Green, J. Pollard, Jr., S. Tugendreich, Causal analysis approaches in Ingenuity Pathway Analysis. *Bioinformatics* **30**, 523-530 (2014); published online EpubFeb 15 (10.1093/bioinformatics/btt703).
76. W. Stauffer, H. Sheng, H. N. Lim, EzColocalization: An ImageJ plugin for visualizing and measuring colocalization in cells and organisms. *Sci Rep* **8**, 15764 (2018); published online EpubOct 25 (10.1038/s41598-018-33592-8).
77. B. A. Walter, O. M. Torre, D. Laudier, T. P. Naidich, A. C. Hecht, J. C. Iatridis, Form and function of the intervertebral disc in health and disease: a morphological and stain comparison study. *J Anat* **227**, 707-716 (2015); published online EpubDec (10.1111/joa.12258).

Acknowledgments:

We thank Monica Garcia-barros and the Biorepository and Pathology CoRE at the MSSM for the assistance and contribution of the immunohistochemistry quantification using the HALO software. We thank Dr. Nadine Schrode for her assistance and insights on the scRNA-seq analysis. We thank Dr. Nilsson Holguin for useful discussions on interpretations.

Competing interests: Authors declare that they have no competing interests.

Figure Legends:

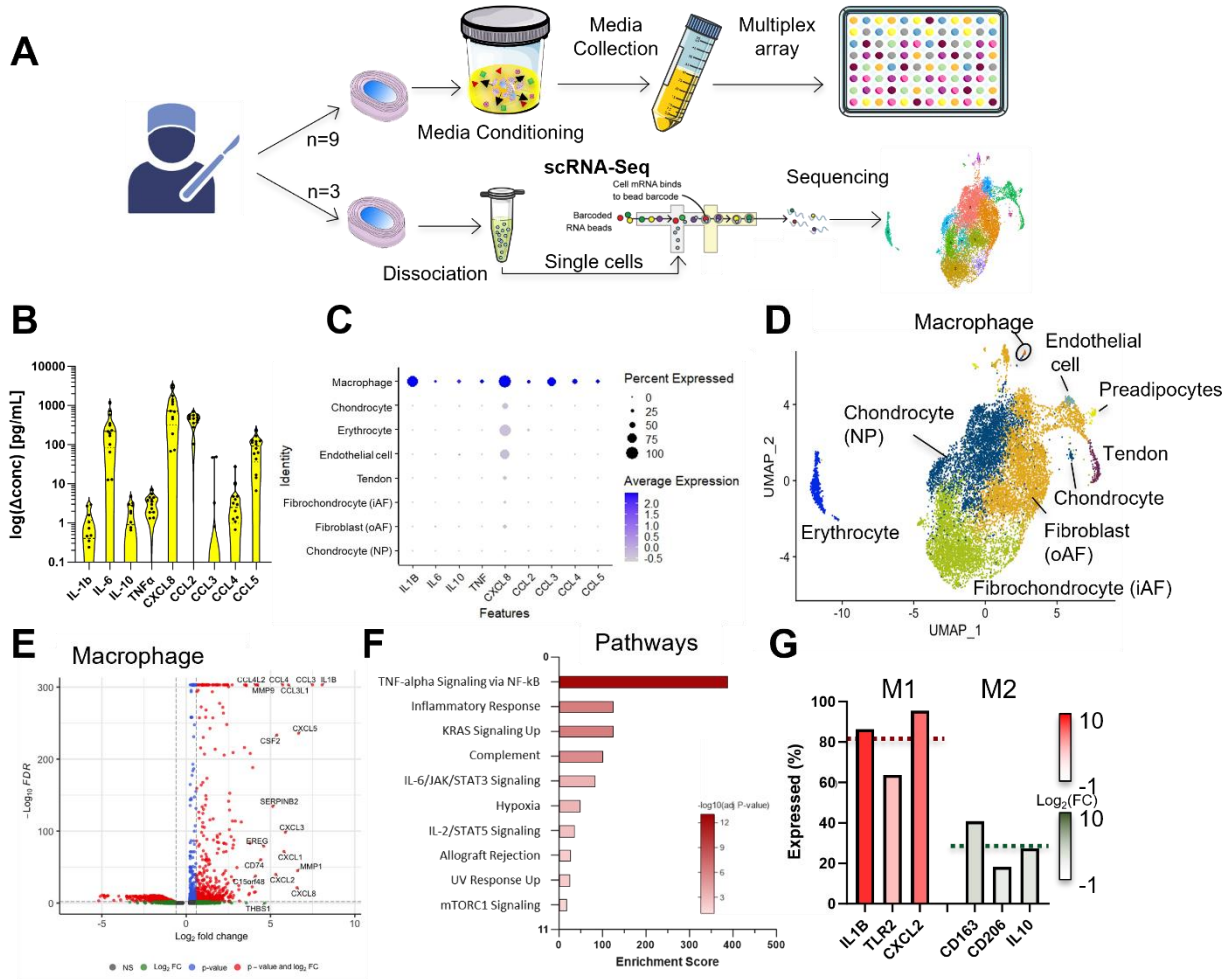

Fig. 1. Cytokines present in human herniated IVDD samples are complex and dominantly expressed from a small population of M1 macrophages highly enriched for TNF-alpha signaling. (A) Specimen from subjects were collected and either used for CM generation and characterization (top) or for cell dissociation and scRNA-seq analysis (bottom). **(B)** IVDD CM contains a complex array of pro- and anti-inflammatory cytokines and chemokines. **(C)** IVDD cytokines are dominantly expressed by macrophage sub-population of IVD cells with surprisingly little expression in other IVDD cell populations. **(D)** UMAP of IVDD cells annotated with UniCell Deconvolve identified 7 cell types including a small population of macrophages. Since relatively few IVD studies are included in the UniCell Deconvolve training set, we parenthetically added IVD-specific annotations to the UMAP. **(E)** Volcanoplot shows DEGs with pro-inflammatory genes CCL3, CCL4 and IL1B as most significantly upregulated genes, which contribute to **(F)** pathways analysis revealing TNF-alpha signaling as the most significant and highest enriched

pathway of this population. **(G)** M1/M2 macrophage polarization quantification showed a 3-fold higher amount of M1 macrophages within the IVD.

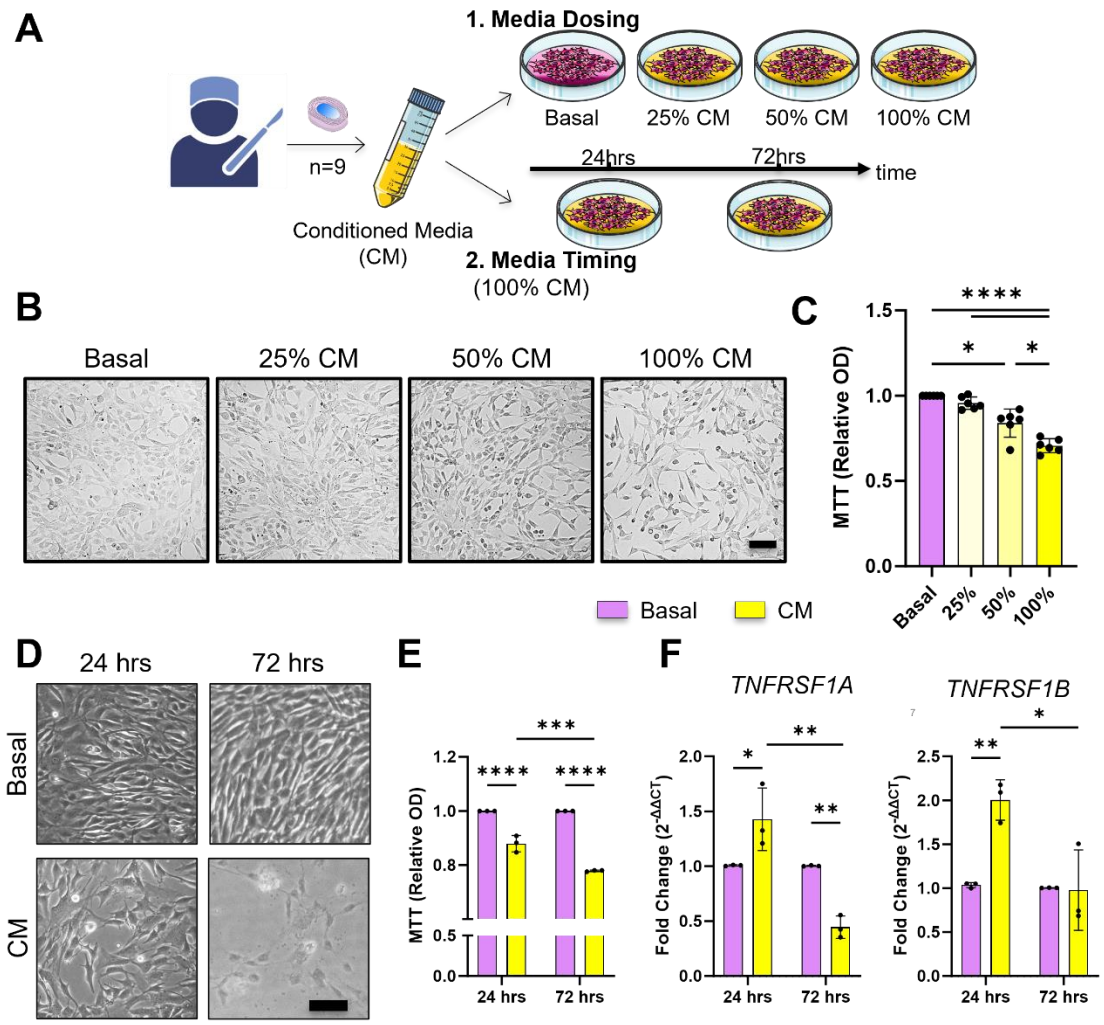

Fig. 2. Human AF cell IVDD model system shows IVDD CM reduces MTT metabolic activity and modulates TNFR1 and TNFR2 responses (A) CM generated from 9 subjects were first applied in different dosages (0-100%) for 24 hours ("Media Dosing"), followed by culture for 24 hours and 72 hours respectively ("Media Timing") **(B)** Cell growth area decreases with increasing concentration of CM, which is reflected in **(C)** where cell proliferation significantly decreases with increasing CM, indicated by MTT assay. **(D)** Culturing hAF cells for 72 hours in CM has a detrimental effect on cell growth and morphology compared to Basal and 24 hours CM exposure, which is also seen in **(E)** with significantly lower relative OD, indicating lower cell growth. **(F)** culture in CM for 24 hours significantly increases gene expression of TNFR1 and TNFR2 compared to Basal control and 72 hours culture. *, **, *** and **** represent significant differences between groups with $p < 0.05$, 0.01, 0.001 and 0.0001 respectively. Scale bar = 100 µm

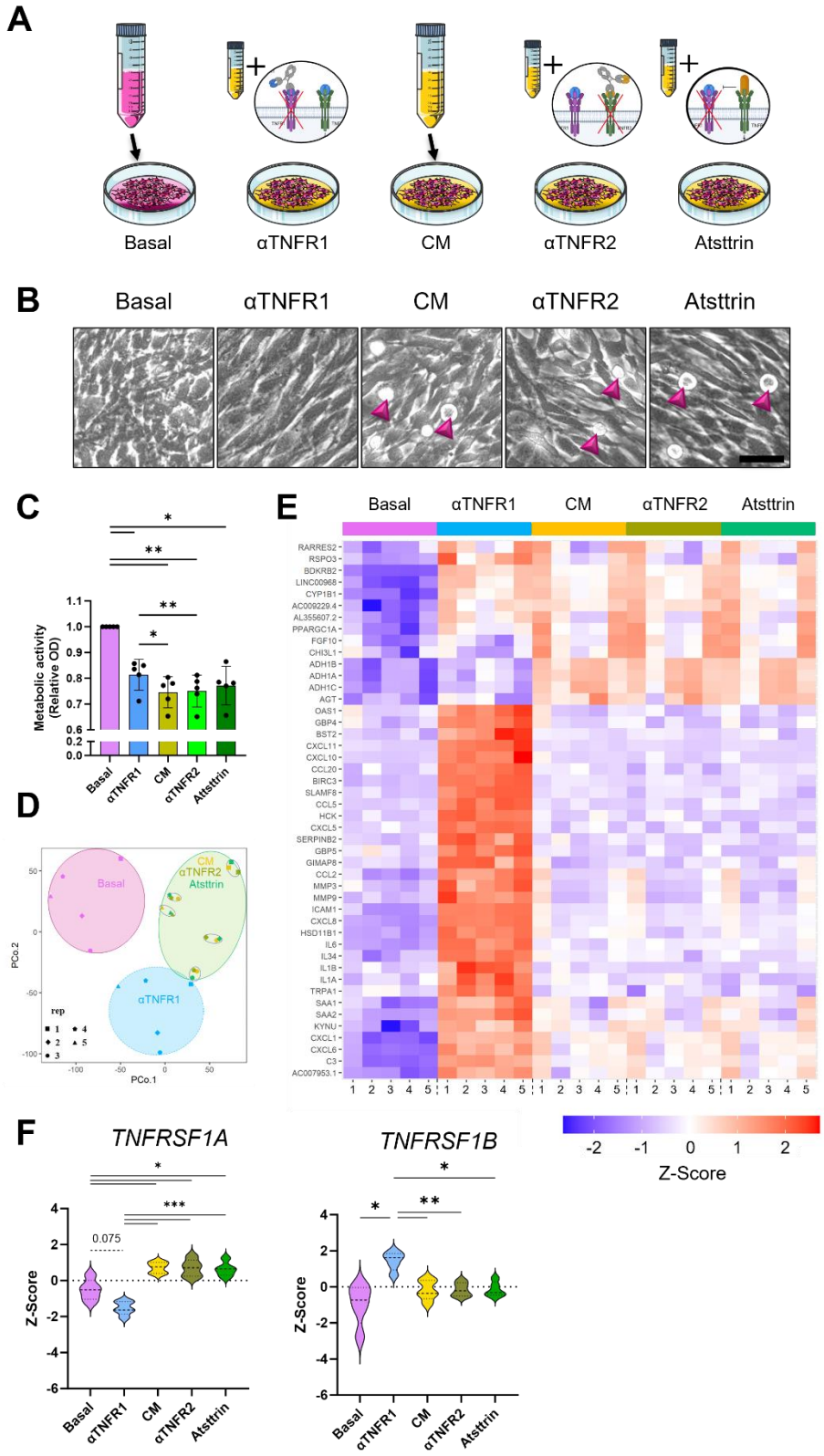

Fig. 3. TNFR1 blocking of hAF cells with IVDD CM partially rescued metabolic rate and drastically changes the transcriptome while TNFR2 blocking and Atsttrin had no

effects. (A) Cells were either cultured for 24 hours in Basal media, CM or CM supplemented with αTNFR1, TNFR2 or Atsttrin respectively. **(B)** hAF cells in CM, αTNFR2 and Atsttrin show greater number of floating dead cells (arrowheads), which is consistent with **(C)** reduced cell growth/viability in CM, αTNFR2 and Atsttrin compared to basal, which was partly recovered in αTNFR1. **(D)** Distinct transcriptomic difference between Basal, αTNFR1 and all other groups are apparent in PCA plot, and **(E)** heatmap, which shows a clear change in top DRG patterns with many pro-inflammatory genes among the top 50 DEGs. **(F)** Gene expression of TNFR1 is significantly downregulated upon TNFR1 blocking, whereas TNFR2 is upregulated. *, ** and *** represent significant differences between groups with $p < 0.05$, 0.01 and 0.001 respectively. Scale bar = 50 µm

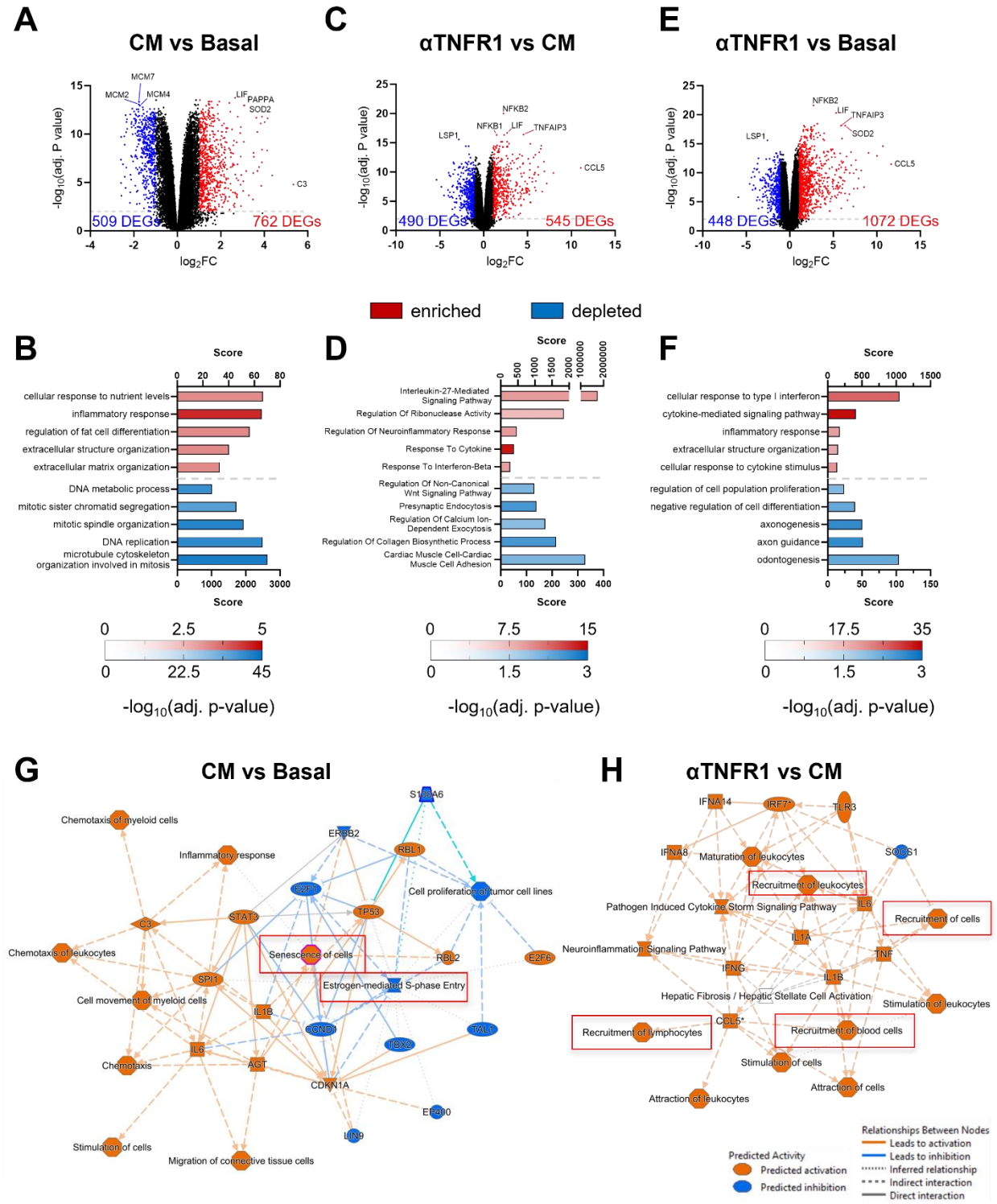

Fig. 4. CM increases inflammation and reduces mitotic responses while TNFR1 inhibition promotes processes for immune cell recruitment. (A) 509 of 1271 DEGs in CM were significantly downregulated compared to Basal. **(B)** Biological processes depleted upon CM were related to DNA replication and mitosis. **(C)** Comparing αTNFR1 to CM, 454/1035 DEGs were significantly upregulated. **(D)** Biological processes modulated by

αTNFR1were related to an enrichment of IL-27 signaling and RNase activity. **(E)** Volcano plot comparing αTNFR1 to Basal significantly upregulated 1072/1520 DEGs. **(D)** Hereby, biological processes related to cytokine signaling and inflammatory responses were enriched, while axonogenesis and axon guidance was depleted. **(G)** Qiagen IPA analysis of CM vs Basal predicted an activation of senescence while proliferation was inhibited. **(H)** Inhibition of TNFR1 activates processes related to immune-cell recruitment in IPA analysis.

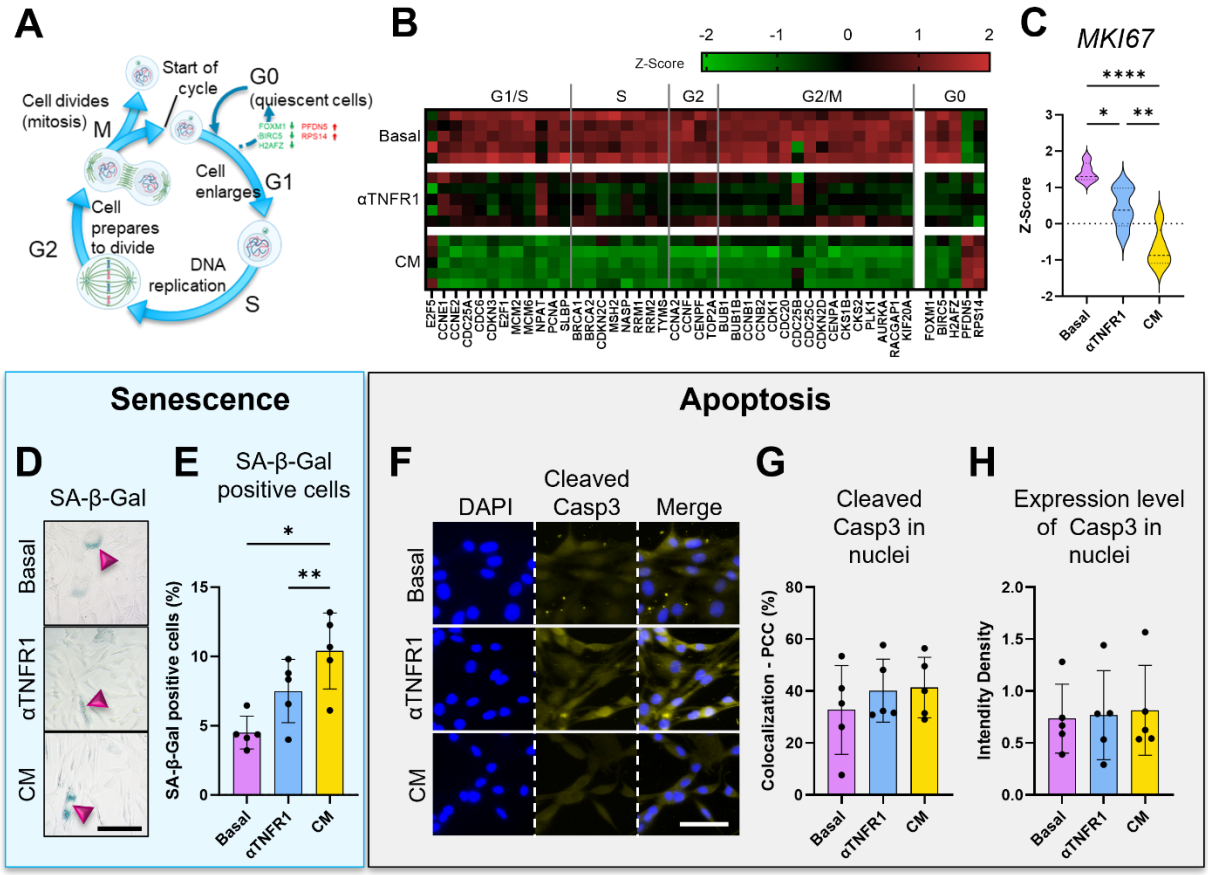

Fig. 5. IVDD CM inhibited active hAF cell mitosis and promoted senescence that was partially prevented with TNFR1 inhibition. (A) Schematic of different stages of the cell cycle which are **(B)** activated in hAF cells cultured in Basal media, while CM cells express genetic pattern of G0 phase. **(C)** MKI67 proliferation marker is significantly decreased in CM compared to Basal and αTNFR1. **(D)** SA-β-Gal staining of hAF cells showed **(E)** significantly higher number of SA-β-Gal positive cells in CM compared to Basal and αTNFR1. **(F)** Staining for cleaved Casp3 showed **(G)** no difference in co-localization of cleaved Casp3 and DAPI and **(H)** no difference nuclear cleaved Casp3 intensity density. *, ** and **** represented p< 0.05, 0.01 and 0.0001, respectively. Scale bar = 50 µm

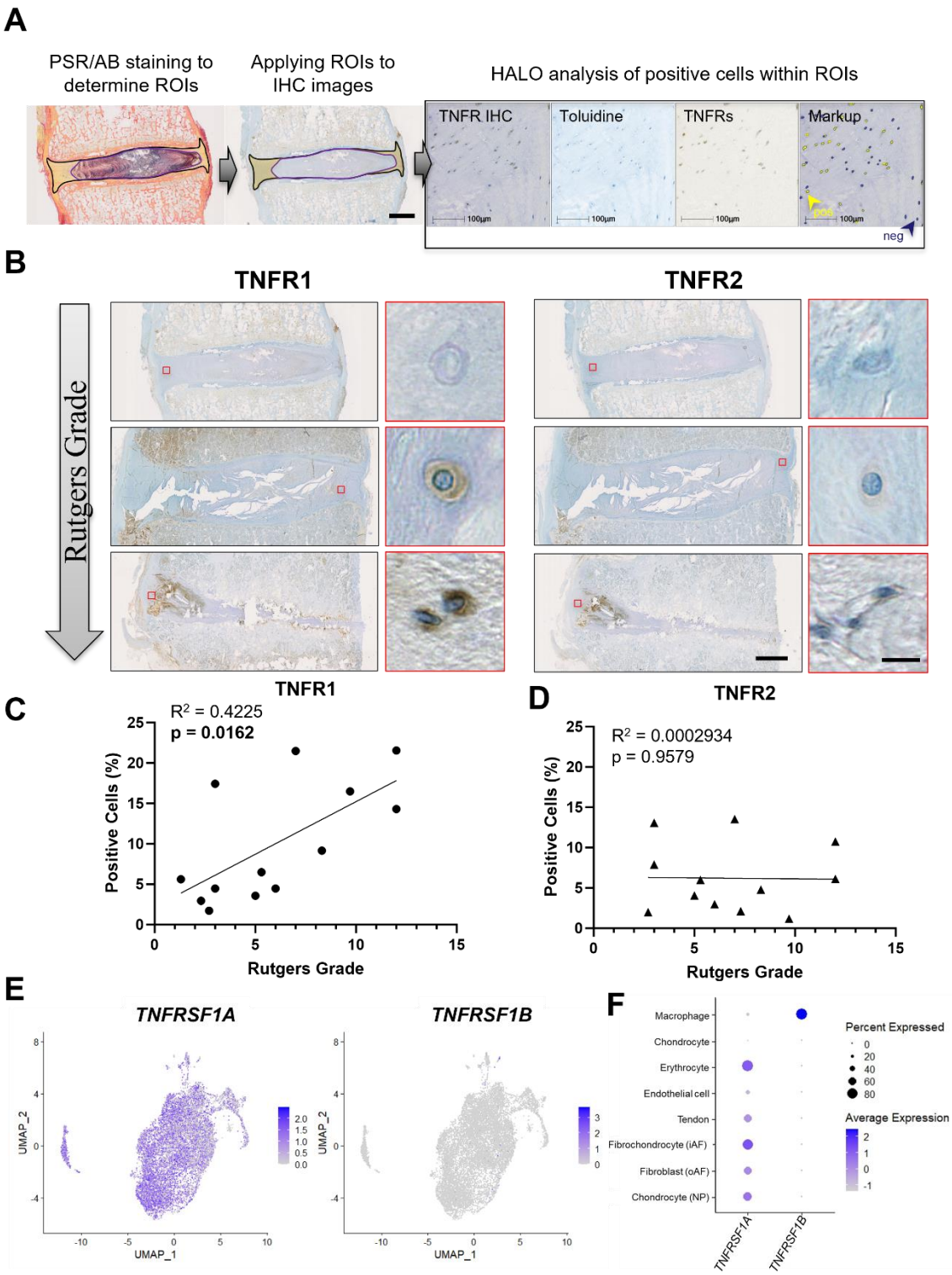

Fig. 6. TNFR1 expression was expressed in all IVD cells and correlated with IVD degeneration grade while TNFR2 was only expressed in macrophages and not IVD cells, highlighting the reduced repair capacities of IVD cells. (A) Analysis of IHC was performed using HALO Multiplex module, whereby the oAF region was determined using

PSR/AB staining and the ROI overlayed onto TNFR1/2 IHC imaged for follow up AI-based analysis. **(B)** Intensity and quantity of TNFR1 increases with Rutgers degeneration grade, while TNFR2 shows faint staining across degeneration. **(C)** Correlation between TNFR1 positive cells and Rutgers grade is significant (p=0.0162), while **(D)** there is no correlation with TNFR2 positive cells and Rutgers grade**. (E)** UMAP of herniated IVD specimen showed TNFR1 expression across cell populations and little TNFR2 expression**. (F)** TNFR2 is expressed exclusively in macrophage-derived cell population. Scale bar (full IVD) = 5 mm, Scale bar (AF cell) = 10 µm

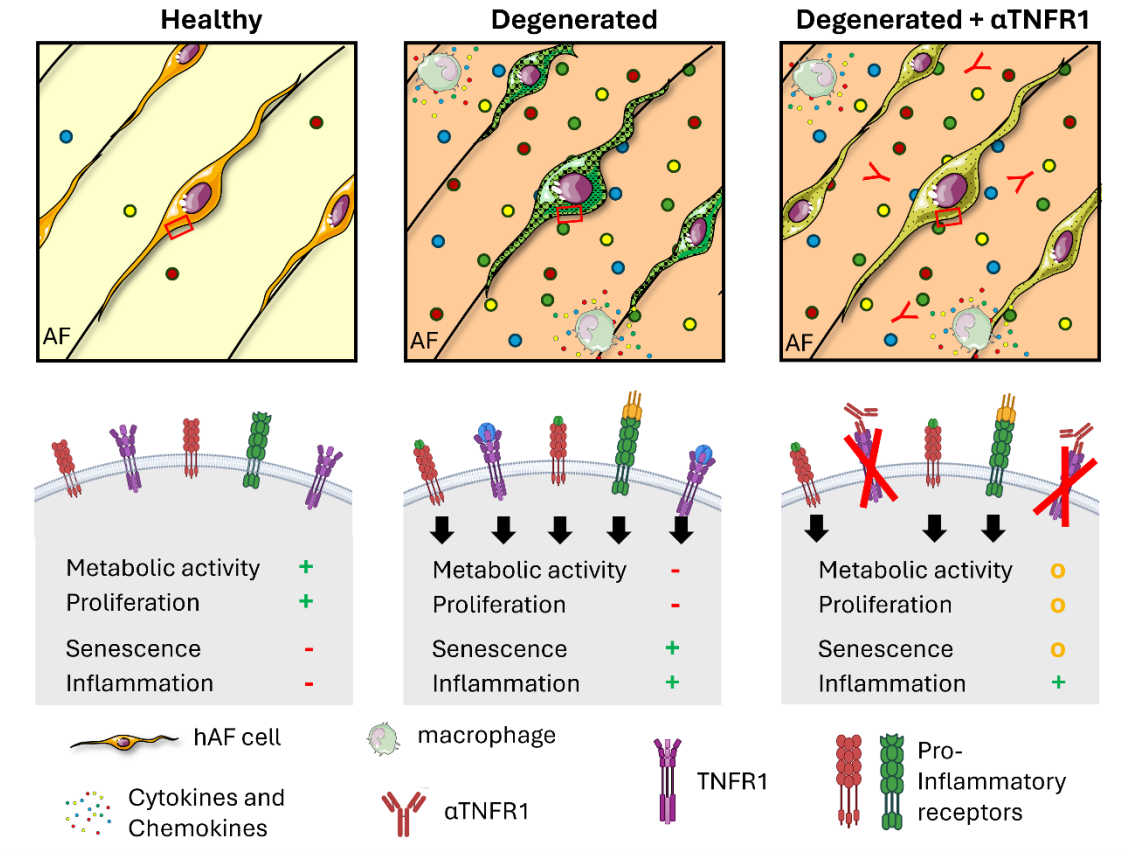

Fig. 7. Summary schematic displaying the anti-proliferative and pro-senescence response of hAF cells towards the cytokine challenge of painful IVDD conditions and the capacity of TNFR1 inhibition to partially recover this response. Lack of TNFR2 on IVD cell membrane limits their repair capacity. In part created with BioRender.com

Table 1. Experimental groups and supplements of individual experiments

	Groups and supplements		Duration
Dosing	Basal	-	24 hours
	CM	25% 50% 100%	
Timing	Basal	-	24 hours 72 hours
	CM	100%	
TNFR blocking	Basal	-	24 hours
	CM	-	
	CM + αTNFR1	10 µg/mL	
	CM + αTNFR2	10 µg/mL	
	CM + Atsttrin	200 ng/mL	